Applied Catalysis B: Environmental 181 (2016) 298–313

Contents lists available at ScienceDirect

Applied Catalysis B: Environmental

journal homepage: www.elsevier.com/locate/apcatb

Review article

Structural parameters of supported fuel cell catalysts: The effect of particle size, inter-particle distance and metal loading on catalytic activity and fuel cell performance

Ermete Antolini*

Scuola di Scienza dei Materiali, Via 25 aprile 22, 16016 Cogoleto, Genova, Italy

ARTICLE INFO

Article history:
Received 16 May 2015
Received in revised form 26 July 2015
Accepted 4 August 2015
Available online 6 August 2015

Keywords:
Polymer electrolyte membrane fuel cell
Catalyst
Particle size
Inter-particle distance
Metal loading

ABSTRACT

Carbon supported platinum is commonly used as anode and cathode catalyst in low-temperature fuel cells. The need of modify the chemical characteristics of the supported catalyst has emerged due to several factors, such as reducing the price of the active catalyst and increasing its activity, selectivity, and long-term stability. Thus, pure Pt is now rapidly being replaced by oxide promoted Pt and Pd or Pt- and Pd-based alloy catalysts in low-temperature fuel cells. In addition to the chemical characteristics of the catalysts, many studies on nanocatalysts have been addressed to correlating the catalytic activity with some physical characteristics of supported fuel cell catalysts. This review article examines the role played by metal particle size, inter-particle distance and metal loading on the support in determining the catalytic activity of supported catalysts.

© 2015 Elsevier B.V. All rights reserved.

Contents

1. Introduction 298
2. Particle size effect 299
   2.1. Principles 299
   2.2. Particle size effect on the activity for oxygen reduction 300
   2.3. Particle size effect on the activity for methanol oxidation 302
3. Inter-particle distance effect 304
   3.1. Principles 304
   3.2. Shielding or diffusion effect (negative effect on the catalytic activity) 304
   3.3. Electrochemical double layer potential drop (Pt oxide reduction peak potential increase) (positive effect on the catalytic activity) 305
4. Metal loading (catalyst layer thickness) effect 307
5. Effect of the link between Me/*S*, *d* and x_i on the catalytic activity 309
5. Conclusions 311
   References 312

1. Introduction

Low-temperature fuel cells, fuelled with either hydrogen (phosphoric acid fuel cell, PAFC, and polymer electrolyte membrane fuel cell, PEMFC), or low molecular weight alcohols (direct alcohol fuel cell, DAFC) are environmentally friendly devices to produce electricity by direct electrochemical conversion of hydrogen/alcohol and oxygen into water/water, carbon dioxide and other alcohol oxidation products [1–3]. Platinum is the best known pure metal electro-catalyst for hydrogen and low molecular weight alcohols oxidation and oxygen reduction in acid medium. To maximise its surface area, platinum is dispersed on a conductive support as carbonaceous materials [4]. Carbon supported platinum is commonly used as anode and cathode catalyst in low temperature fuel cells [4]. Pure Pt, however, is not the most effective anode catalyst for PEMFCs fuelled with reformate gas (H_2/CO) and DAFCs. Indeed, platinum is rapidly poisoned on its surface by strongly adsorbed CO and, in the case of DAFCs, by alcohol oxidation intermediate species.

* Corresponding author. Fax: + 39 010 918 23689.
E-mail address: ermantol@libero.it

http://dx.doi.org/10.1016/j.apcatb.2015.08.007
0926-3373/© 2015 Elsevier B.V. All rights reserved.

Efforts to mitigate the poisoning of Pt have been concentrated on both the addition of cocatalysts, particularly ruthenium and tin, to platinum [5,6] and the use of Pt-free catalysts [7,8]. On the other hand, kinetic limitations of the oxygen reduction reaction (ORR) on pure Pt are a serious drawback, reducing PEMFC performance [9]. To decrease the cathodic cell voltage losses, extensive studies were addressed to the development of ORR catalysts more active than pure Pt. The alloys of transition metals, such as V, Cr, Fe, Co, and Ni, with Pt showed considerably higher electrocatalytic activities towards oxygen reduction than platinum alone in low-temperature fuel cells [10–17].

In addition to the chemical characteristics of the catalysts, such as the type of cocatalyst, platinum to cocatalyst atomic ratio, degree of alloying and non-platinum catalysts, some physical characteristics of supported fuel cell catalysts can deeply influence their catalytic activity. The shape or morphology of Pt nanoparticles provides a powerful tool for tuning its electrocatalytic properties. The shape-dependent properties of nanostructured platinum have been explored, showing that the catalytic activity can be related to the shape of platinum nanostructures [18,19]. Metal particle size (d) and inter-particle distance (x_i) are key parameters influencing the catalytic activity of supported catalysts and, hence, fuel cell performance. Moreover, metal loading (Me/S), that is, the amount of metal present on the support, affecting the thickness of the fuel cell catalyst layer, also influence cell performance. These parameters are strictly correlated: indeed for the most part of synthesis methods d depends on Me/S, while x_i always depends on both d and Me/S. A schematic representation of the link between Me/S, d and x_i and their effect on catalytic activity and fuel cell performance is shown in Fig. 1. In this review the role played by metal particle size, inter-particle distance and metal loading on the support in determining the catalytic activity of supported catalysts is analyzed.

2. Particle size effect

2.1. Principles

Generally, the mass activity (MA, activity mass^{-1}) of a catalyst is defined as the current normalised by the noble metal loading or catalyst loading as measured at a specific potential, and can be expressed as:

$$\mathrm{MA} = \mathrm{SA} \times \mathrm{SSA} \quad (1)$$

where SA is the specific activity (activity area^{-1}), defined as the current normalised by the chemical (CSA) or electrochemical (ECSA) surface area and SSA is the specific, chemical or electrochemically active, surface area (area mass^{-1}). To decrease platinum loading of PEMFC electrodes it is necessary to increase MA, which can be improved by increasing the specific surface area of the catalysts, *i.e.*, by decreasing the particle size. However, a lot of papers reported a particle size effect in the oxygen reduction and alcohol oxidation reactions for particle sizes <5 nm, due to the changes of SA with particle diameter. Thus, owing to the size effect, MA is not inversely proportional to particle size, but goes through a maximum. The particle size effect on the specific activity of catalysts has been attributed to different factors, such as the structural sensitivity, that is, the dependence on the geometry of the surface [20–25], the electronic state of the catalyst [26,27], the potential of zero total charge [28] and the metal-support interaction [29]. For cuboctahedral particles, which consist of {1 1 1} and {1 0 0} facets bounded by low coordination number (edge and corner) atoms, simple geometric considerations indicate that the relative concentration of surface atoms on facets or in edge and corner positions changes dramatically as the crystallite size decreases in the 5–1 nm particle range, influencing CO oxidation potential [20]. Perez-Alonso et al. [21] reported that the activity for oxygen reduction decreased with decreasing Pt nanoparticle size, corresponding to a decrease in the fraction of terraces on the surfaces of the Pt nanoparticles. Park et al. [22] reported that the availability of contiguous Pt terrace sites progressively decreases with decreasing particle. The fraction of Pt "flat terrace" *versus* edge sites on the nanoparticle surface decreases sharply for $d \leq 4$ nm. Such structural alterations indicate the progressive reduction in the presence of 9-coordinate terrace sites along with the emerging dominance of lower-coordinate Pt surface atoms, as d decreases from *ca.* 4 to 2 nm. These findings resulted in a nanoparticle-size-dependent electrocatalytic activity for methanol, formic acid and formaldehyde electrooxidation. Greeley et al. [25] used a simple, first-principle based model of the ORR to evaluate ORR kinetics on the {1 1 1}, {1 0 0} and {2 1 1} facets of eleven metals, including Pt. Among almost all these metals, {2 1 1} steps presented lower ORR activity than that of planar terraces: indeed, oxygen reduction intermediate species, such as O and OH radicals, are bound too strongly to the steps, increasing the barrier to form water on these defect sites. These results, combined with simple models of the geometry of nanoparticles, resulted in a decrease of the ORR with decreasing Pt particle size.

The distinct electronic properties of such sites are expected to play a role in chemical reactivity by, for example, facilitating the dissociation of reactants or by stabilizing intermediate reaction species. When the particle size of carbon-supported Pt clusters was <5 nm, a strong adsorption of H, OH and C_1 compounds such as CO on metal particles was observed [26]. The strong adsorption of OH beyond 0.8 V *vs.* RHE on small particles inhibited the reduction of oxygen. Fig. 2 shows a normalized plot of the d-band vacancy/atom *vs.* particle size on going from 0.54 to 0.0 V *vs.* RHE. The changes of the d-band vacancy/atom increased as the particle size was reduced from 7 to 3 nm. The results indicated that the electronic effects due to adsorption of H and OH are larger for the small particles even when the results are normalized to account for the number of surface atoms. Fig. 2 also shows a plot of the change in the Pt–Pt coordination number ΔN for the various Pt particle sizes. In the case of the small particles, strong absorption of H induces morphological changes in the Pt clusters that are reflected in the increased Pt–Pt coordination numbers.

Mayrhofer et al. [28] presented a method for establishing the potential of zero total charge (pztc) as a function of particle size. The values of pztc were invoked to explain the trend for adsorption of oxygenated species, such as OH, on the Pt clusters. Pztc shifts at lower potentials (*ca.* 35 mV) by decreasing the particle size from 30 nm down to 1 nm. As a consequence, the energy of adsorption of OH is enhanced, that is, at the same potential the surface coverage with OH increases by decreasing the particle size, which in turn affects the catalytic reactions.

Finally, the metal-support interaction may also be in part responsible for the change of the specific activity. The smaller Pt particles can have higher fraction of surface atoms interacting with the carbon support than larger particles, enhancing the charge transfer between carbon support and Pt particles, and likely modifying the catalytic activity [29].

Conversely, few works reported no effect of the particle size with small (1–5 nm) high-surface-area particles on the ORR activity of Pt catalysts [30–32], but it was observed that the activity rapidly increases at larger particle sizes, until it reaches that of bulk platinum [31]. Considering that the most part of the experimental results in literature reported a substantial decrease of the ORR specific activity on reducing the particle size in the range 1–5 nm, more work is needed to confirm the absence of a particle size effect in this size range on the catalytic activity.

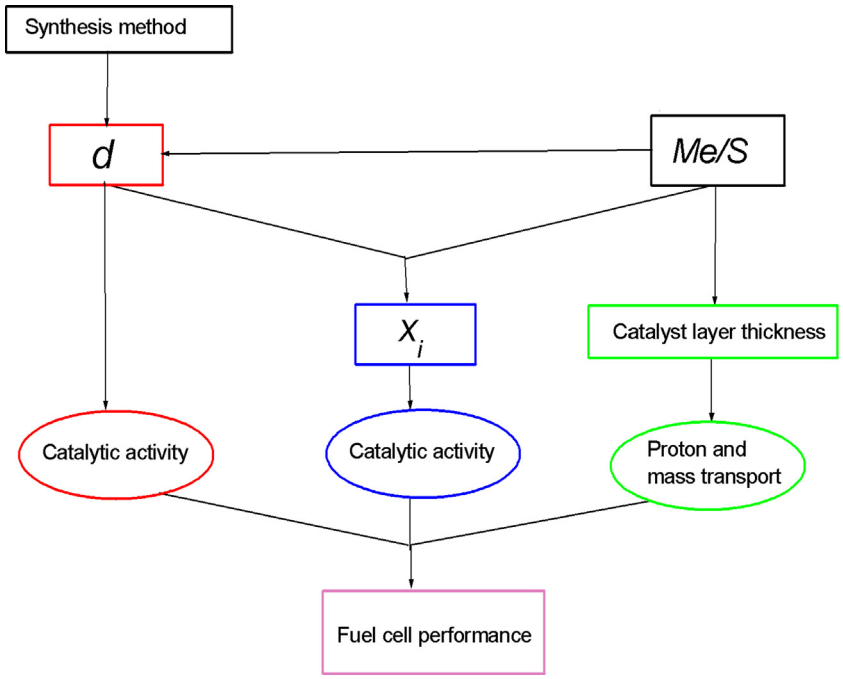

Fig. 1. Schematic representation of the link between Me/*S*, *d* and x_i and their effect on catalytic activity and fuel cell performance. Me/*S*—metal loading; *d*—particle size; x_i—inter-particle distance.

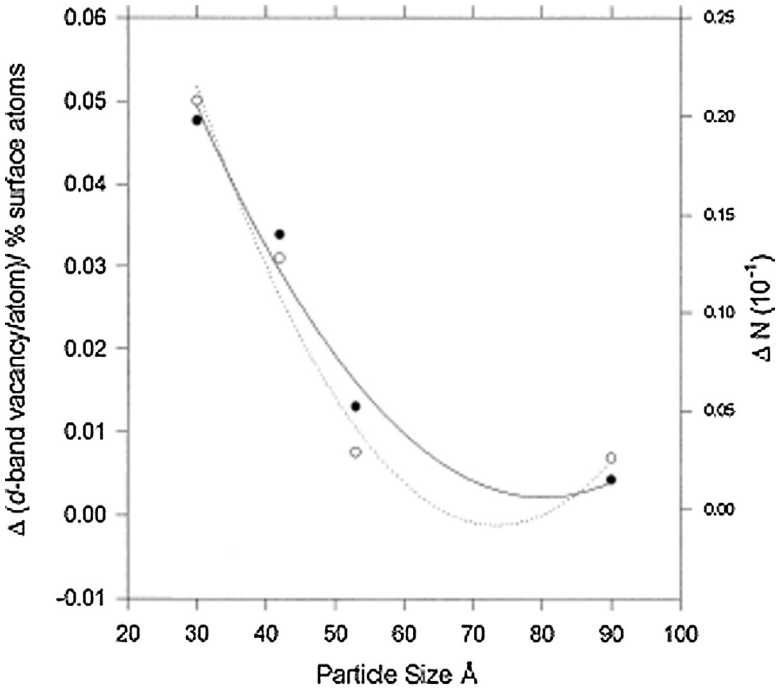

Fig. 2. The effect of particle size on the change in the normalized *d*-band vacancies (*d*-band vacancies/% surface atoms) (· · ·) in going from 0.54 to 0.0 V *vs.* RHE. The change in the Pt–Pt coordination number, as determined from L_3 EXAFS, is also shown (—). Reproduced from Ref. [26], copyright 1998, with permission from Elsevier.

In the following paragraphs we report a literature overview regarding the effect of particle size of Pt and Pt-based binary catalysts on the activity for oxygen reduction and methanol oxidation.

2.2. Particle size effect on the activity for oxygen reduction

In oxygen reduction measurements on platinum electrodes the most commonly used electrolytes are $HClO_4$ and H_2SO_4. In the non-adsorbing $HClO_4$, the ORR activity depends on Pt surface structure and decreases in the order of {1 1 0} > {1 1 1} > {1 0 0} due to the decreased interaction strength between O_2 and different surface structures [33]. For the adsorbing H_2SO_4, instead, the ORR activity decreased in the order of {1 1 0} > {1 0 0} > {1 1 1}, by the adsorption and inhibiting effect of bi-sulfate anion on the {1 1 1} facets [34]. It was suggested that the change in the fraction of surface atoms on the {1 0 0} and {1 1 1} crystal faces of Pt particles, going from smaller spherical to larger cubo-octahedral structures, can be correlated to the specific activity and the mass activity for the ORR

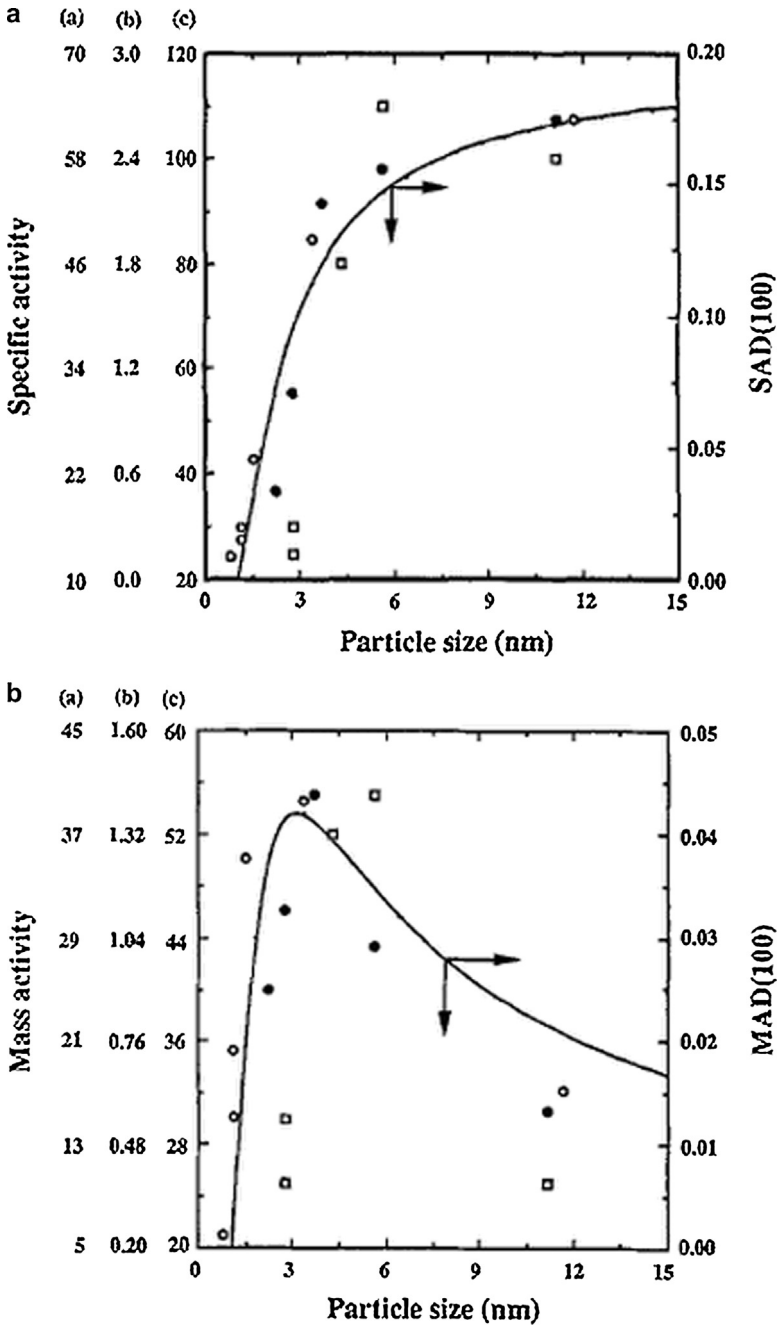

Fig. 3. Superimposed plots of SA (specific activity, normalized to CSA). MA is normalized to metal loading for oxygen reduction and SAD (1 0 0) (surface atom distribution on the {1 0 0} crystal faces, normalized to the total number of atoms on particle surface) (Fig. 3a) and MA (mass activity, normalized to metal loading) for oxygen reduction and MAD (1 0 0) (surface atom distribution on the {1 0 0} crystal faces, normalized to the total number of atoms in the particle) (Fig. 3b) as a function of particle size: (solid line) SAD (1 0 0) (Fig. 3a) and MAD (100) (Fig. 3b). (a) (●), 98% H_3PO_4, 180 °C; (b) (o), 0.5 M H_2SO_4, 25 °C; and (c) (□), 97% H_3PO_4, 177 °C. Reprinted from Ref. [23], copyright 1990, with permission from The Electrochemical Society.

of Pt electrocatalysts. In H_2SO_4 the maximum in mass activity was attributed to the maximum in the surface fraction of Pt atoms on the {1 0 0} crystal face, resulting from the change in surface coordination number with a change in the particle size [23]. The dependence of both the specific activity and the distribution of surface atoms on the {1 0 0} crystal faces, normalized to the total number of atoms on particle surface (SAD (1 0 0)) on the particle size is shown in Fig. 3a. A decrease of both SA and SAD with decreasing Pt particle size can be observed in Fig. 3a. The close agreement between SA and SAD suggested that oxygen reduction on highly dispersed Pt in acid electrolyte is a structure-sensitive reaction. The superimposed plots of the mass activity and the distribution of surface atoms on the {1 0 0} crystal faces, normalized to the total number of atoms in the particle (MAD (1 0 0)) as a function of the particle size is shown in Fig. 3b. The SAD (1 1 1) and MAD (1 1 1) showed similar trends as a function of Pt particle size. The maximum in mass activity was attributed to the maximum in the surface fraction of Pt atoms on the {1 0 0} and {1 1 1} crystal faces, which results from the change in surface coordination number with a change in the particle size [23]. On the other hand, according to Kabbabi et al. [35] and Gamez et al. [36], the origin of the particle size effect was ascribed to the stronger adsorption of oxygenated intermediate species on the smaller particles, which hinders the ORR. As these works [22,34,35] were carried out in H_2SO_4, considering that

sulphate anions can diffuse from aqueous electrolyte across the active layer, the origin of the size effect could be partially due to their adsorption on Pt nanoparticles. Based on structure-activity correlation described by Markovic et al. [33,34], different activity trends would be predicted in different electrolytes. Conversely, the same activity trend found in H_2SO_4, that is, a decrease of SA with decreasing Pt particle size, was also observed in non-adsorbing $HClO_4$ [21,26–28,37–44]. The independence of the activity trend of the electrolyte has to be ascribed to other effects than the type of terraces ({1 0 0} or {1 1 1}), such as Pt electronic state [26,27], the edge sites [38] and the potential of zero total charge [28,40], resulting in a stronger interaction of oxygenated species with smaller Pt particles. Takasu et al. [27] attributed the particle size effects on the ORR to stronger interaction of oxygen with smaller Pt particles, due to the dependence of Pt electronic state on particle size. XPS measurements showed that the binding energy of the $Pt4f_{3/2}$ and $P4f_{5/2}$ states for Pt particles on a glassy carbon electrode shifts to a higher value with decreasing Pt particle size. So, the interaction between the adsorbed oxygen species and surface platinum atoms should be stronger with decreasing Pt particle size, as the energy separation between the highest occupied energy level for oxygen and platinum valence bands decreases with decreasing Pt particle size. A similar conclusion was reported from in-situ XAS measurements by Mukerjee and Mc Breen [26]. Shao et al. [39] evaluated the dependence of SA and MA on Pt particle size in the range of 1–5 nm. The specific activity increased fast by 4-fold as the particle grows from 1.3 nm to 2.2 nm, then increased slowly as particle size further increases. These results were explained by density functional theory (DFT) calculations performed on fully relaxed nanoparticles. The presence of the edge sites is the main reason for the low specific activity in nanoparticles due to very strong oxygen binding energies at these sites. The contribution of {1 1 1} facets to overall specific activity becomes smaller in particles as their size decreases. Much higher binding energy at edge sites than at {1 1 1} facets indicates that the rate determining step for these sites is desorption of intermediates. Because of the strong reactivity of edge sites, it can be concluded that these sites are blocked by adsorbed intermediates during the ORR. This explains the sharp drop of the specific activity. The geometric models [34,39], however, are not sufficient to describe the particle-size effect for large particles and the higher SA activity of bulk Pt than that of carbon supported Pt catalysts observed in some works [28,31,37,38]. This could to be ascribed to effects related to the non-ideal shape of real catalysts, the mass transport of oxygen within micropores, the catalyst support and the inter-particle distance [45]. Another way to explain both the small and the large particle effect on the ORR activity is the dependence of the potential of zero total charge (pztc) on particle size [28,40]. Mayrhofer et al. [28,40] compared the ORR activity on an extended Pt surface and on Pt nanoparticles. SA increased with increasing particle size, independently of the temperature or the potential in the kinetic region. Owing to the decrease of particle size and the associated decrease of the average coordination number of atoms, the potential of total zero charge shifted negatively from 0.285 V for polycrystalline Pt and 0.282 V for a nanostructured Pt film to about 0.245 V for carbon-supported Pt nanoparticles with a mean diameter of 1.25 nm. So, the energy of adsorption of anions, in particular OH, was enhanced, that is, at the same potential the surface coverage by oxygenated species increased by decreasing the particle size. The high oxophilicity of smaller particles resulted in a SA decrease, due to the blocking of the active sites required for the adsorption of O_2 or the splitting of the OO bond.

The optimum crystallite size for the ORR, expressed as mass activity, on polycrystalline Pt nanoparticles was in the range 2–4 nm [23,39,41–43,46].

Considering the excellent agreement observed between the ORR activities measured in $HClO_4$ and by PEMFC testing, Gasteiger et al. [47] affirmed that the same particle size effects would occur in PEMFCs. For this purpose, Xu et al. [48] tested Pt/C electrocatalysts with particle size in the range 2.9–6.5 nm as PEMFC cathode materials. A clear particle size effect on the ORR activity and the electrochemical stability was observed, ascribed to the decrease of surface defects with increasing the particle size. SA increased with increasing the particle size, while MA went through a maximum at a particle size value of *ca.* 4 nm.

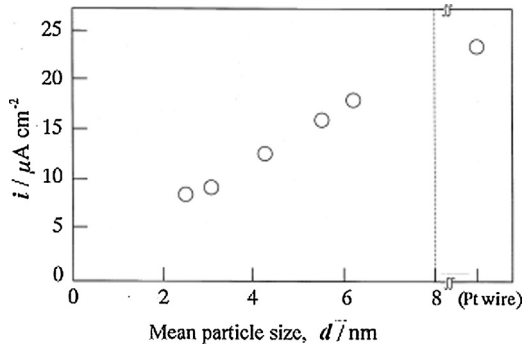

Fig. 4. The relationship between the quasi-steady state current density of the platinum wire and Pt/GC electrodes for the oxidation of methanol and the mean particle size of platinum. Electrolyte: 0.02 M $HClO_4$ + 0.1 M CH_3OH solution, 25 °C. The current density was determined 10 min after setting the electrode potential at 0.60 V from 0.05 V *vs.* SHE during the chronoamperometry. The real surface area of the electrodes was determined from the charge used for the electrochemical oxidation of monolayer-adsorbed carbon monoxide on the platinum sites of the electrodes. Reproduced from Ref. [51], copyright 2000, with permission from Elsevier.

A particle size effect was observed also on the average number of exchanged electrons in the ORR. The average number decreased, and the H_2O_2 formed increased with decreasing the particle size [49].

2.3. Particle size effect on the activity for methanol oxidation

The electrochemical oxidation of methanol on platinum is more complex than oxygen reduction. The methanol oxidation reaction (MOR) proceeds through two main pathways, that is, by CO oxidation (serial pathway), and by the oxidation of other reactive intermediates (parallel pathway) [50]. The multiple site mechanism, where the oxidation of methanol adsorbate on the Pt surface by an oxygenated species adsorbed on the adjacent Pt site is a rate-determining step, is widely accepted. Thus, a balanced co-adsorption of methanol and water onto Pt surfaces is a key factor for a high activity of the MOR catalysts. The particle size effect on the MOR has been studied by several investigators, and it has been reported that, generally, analogously to the oxygen reduction, for $d \leq 5$ nm the specific activity for methanol oxidation decreases with decreasing particle size [22,26,35,43,51–55]. Fig. 4 shows the relationship between the current density for methanol oxidation of the platinum wire and the carbon supported Pt electrodes and Pt particle size [51]. The platinum wire electrode shows the highest specific activity, expressed at the steady state current density at 0.6 V *vs.* SHE, then a decrease of the SA occurs with decreasing platinum particle size. The decrease of the MOR activity with decreasing particle size was ascribed to the increase of the adsorption strength of oxygenated species on Pt, limiting the adsorption of methanol species [35,52,53], and to the stronger adsorption of poisoning species, such as CO, on the smaller Pt particles [53,54]. Maillard et al. [55] suggested that the size effect on SA could be due by the restricted mobility of adsorbed CO at small Pt nanoparticles. From FT-IR spectroscopy and voltammetry, Park et al. [22] deduced that the dependence of the CO adsorption and the electrocatalytic activity on particle size are related to the occurrence of a Pt site "ensemble effect", where methanol dehydrogenation,

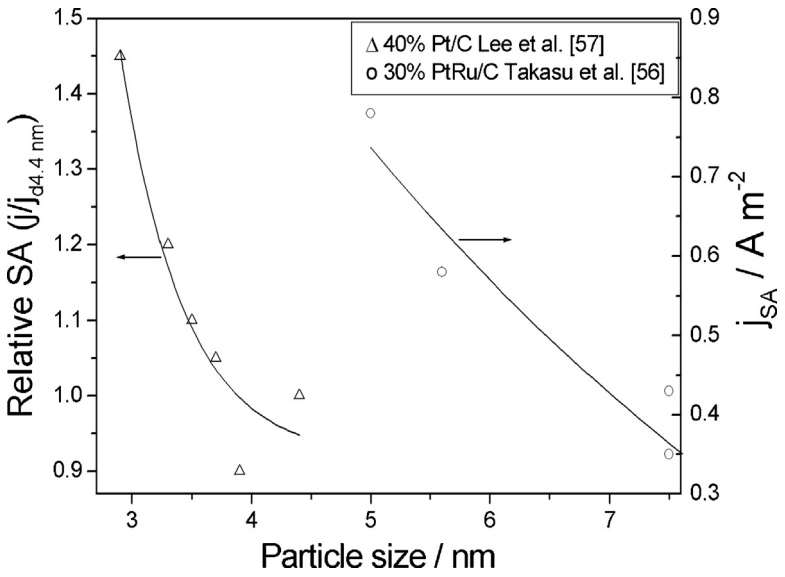

Fig. 5. The dependence of the MOR specific activity of PtRu/C [56] and relative specific activity of Pt/C [57] on metal particle size. Carbon black supports: (o) Mitsubishi; (Δ) Vulcan XC 72R.

to form CO and reactive intermediates leading to CO_2 formation, is hindered by the decreasing availability of contiguous Pt terrace sites for $d < 4$ nm. A maximum in mass activity for the MOR was observed at d values of *ca.* 1.8 nm [52] and 2.5 nm [42].

Conversely, some works reported an opposite effect of particle size on the MOR activity [56–58]. As can be seen in Fig. 5, for both high [56] and low [57] particle size, the specific activity for methanol oxidation increases with decreasing particle size. The increase of MOR activity with decreasing particle size was ascribed to the high ability of small particles to oxidise adsorbed CO and COH intermediates by the high amount of adsorbed OH at a lower overpotential [57,58]. This result is in agreement with that of Mayrhofer et al. [28], which studied the particle size effect on the formation of OH adlayer and the CO bulk oxidation. Based on the negative shift of the potential of total zero charge by decreasing the particle size, the energy of adsorption of OH is enhanced, that is, at the same potential the surface coverage with OH increases by decreasing the particle size. The effect of the potential shift on the OH adsorption is revealed by the CO bulk oxidation reaction, promoted by adsorbed OH.

An intermediate dependence of the specific activity for the MOR on particle size with respect to previously reported results was observed firstly by McNicol et al. [59]. They found that the MOR activity of platinum initially increases, then decreases with increasing Pt particle size, thus giving rise to a maximum in the activity-particle size relationship. More recently, Yoo et al. [60] found that the dependence of the specific activity for methanol oxidation on PtRu particle size goes through a maximum. The oxophilicity, which increases by decreasing the particle size either promotes the methanol oxidation reaction or blocks the surface sites required for the adsorption of CH_3OH. When the adsorbed OH acts as a promoter of a reaction, as in the case of the oxidation of CO on PtRu, the increase in the oxophilicity with decreasing particle size results in an increase in the MOR specific activity. On the other hand, the increase in the oxophilicity in the case of the smallest particles leads to a decrease in the specific activity, because the high amount of OH groups can effectively block the active sites required for the adsorption of CH_3OH. When the ability of the PtRu to bind OH is not too weak and not too strong, a maximum in the catalytic activity is attained, at a PtRu particle size of 2.3 nm, as shown in Fig. 6. The same dependence of the specific activity for ethanol

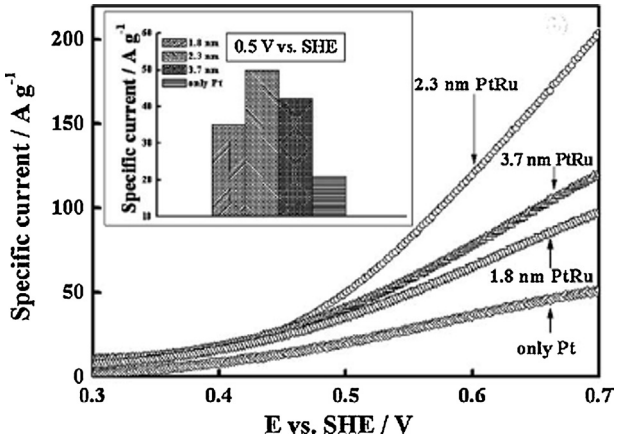

Fig. 6. Polarization curves for the oxidation of methanol on the 1.8–3.7 nm PtRu/TiO_2 nanocatalysts deposited on the glassy carbon electrodes in 0.1 M $HClO_4$ + 2 M CH_3OH at 25 °C; the sweep rate was 50 mV s^{-1}. Reproduced from Ref. [60], copyright 2010, with permission from Elsevier.

oxidation on Pt particle size, going to a maximum at 2.6 nm, was observed by Perez et al. [61].

A particle size effect on the methanol tolerance of oxygen reduction electrocatalysts was observed by Maillard et al. [43]. As can be seen in Fig. 7a, the ORR specific activity in the absence of methanol decreases with a decrease in Pt particle size from 3.4 to 2.3 nm. On the other hand, the MOR specific activity remarkably decreases for the smaller Pt particles ($d < 2.3$ nm), whereas it is approximateley independent of the particle size for $d > 3$ nm. As a result, a maximum in mass activity for both oxygen reduction and methanol oxidation is observed for d about 2.7 nm (Fig. 7b). Following methanol addition, a considerable decrease of the ORR specific activity at the Pt/C catalysts is observed (Fig. 7a). Differently from what observed in the absence of methanol, SA for oxygen reduction in the presence of methanol increases with a decrease of the Pt particle size, (Fig. 7a). From the SA results, it follows that MA for oxygen reduction in the presence of methanol monotonously increases with decreasing Pt particle size (Fig. 7b), attesting a remarkable particle size effect on the methanol tolerance.

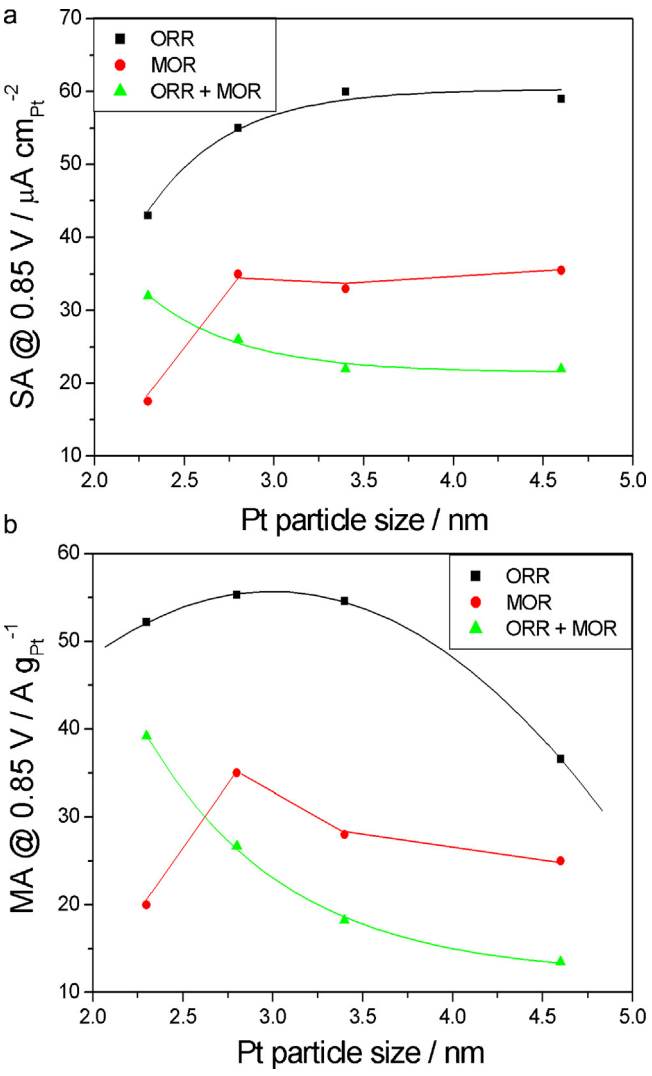

Fig. 7. Specific activity (SA) (Fig. 7a) and mass activity (MA) (Fig. 7b) as a function of the Pt particle size. (■) O_2-saturated 0.1 M $HClO_4$; (●) N_2-purged 0.1MHClO$_4$ with 0.1 M CH_3OH; (▲) O_2-saturated 0.1 M $HClO_4$ with 0.1 M CH_3OH. SA and MA were calculated at 0.85 V *vs.* RHE. Reproduced from Ref. [43], copyright 2002, with permission from Elsevier.

3. Inter-particle distance effect

3.1. Principles

The center to center distance between two adjacent particles is defined inter-particle distance (x_i). For the calculation of x_i it is assumed that all particles exhibit a spherical shape, are monodispersed and homogenously distributed on the carbon support. Generally, the effect of x_i on the catalytic activity is considered negligible, but this assumption is not always true. When the particles are close together within some critical region, a mutual influence takes place. While a lot of work have been addressed to the effect of catalyst particle size on the electro-catalytic activity [20–61], relatively few and conflicting results have been reported on the effect of x_i on the catalytic activity of fuel cell catalysts [35,62–72]. To explain the effect of x_i on the catalytic activity of supported catalysts, two different models were proposed, both supported by experimental results, one based on the shielding or diffusion effect of close particles, (presenting a negative effect on the catalytic activity), and the other on the Pt oxide reduction peak

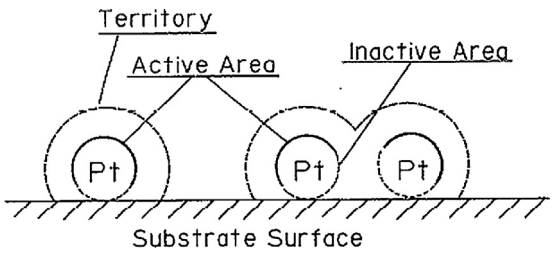

Fig. 8. Territories of supported catalyst particles relating to reactants. Reproduced from Ref. [62], copyright 1989, with permission from Elsevier.

potential increase with decreasing x_i (having a positive effect on the catalytic activity).

3.2. Shielding or diffusion effect (negative effect on the catalytic activity)

An influence of spherical diffusion at the particle level and possible interaction between particles was reported [62,63]. This shielding effect is schematized in Fig. 8, where it can be seen that when a Pt particle is well separated from a neighbor Pt particle, the full surface area is utilized for the ORR, and the O_2 molecule is undergoing spherical diffusion to the individual crystallites. When Pt particles are close together within some critical region, there is a mutual influence on the diffusion, or some other parameter, such that the whole area is not available. They called this critical region "territories of supported catalyst particles relating to reactants". More than the x_i value, however, the inter-particle distance to particle size ratio (x_i/d) seems to be the key parameter affecting the catalytic activity of supported catalysts [36,63]. The diffusion and/or the shielding effect of inter-particle distance should be accounted for when the particles are very close together (*i.e.*, x_i/d between about one and five) [36]. In other words, with the decrease of x_i/d, the diffusion characteristics changes from the spherical diffusion of isolated Pt nanoparticles to an about planar diffusion typical of Pt films, neglecting the curvature of the support for small regions of carbon surface [73]. The role and contribution of transport processes in electrocatalytic reactions was investigated in model studies of the oxidation of CO, using monodispersed, uniformly distributed platinum nanostructures (100–140 nm diameter) supported on glassy carbon [73]. Transport effects were investigated by changing the density of the nanostructures and the electrolyte flow. The identical mass transport limited current observed for the medium and higher coverage nanostructured electrodes and the Pt film electrode showed that the CO transport to the array of Pt nanodiscs takes place by planar diffusion (or 'vertical diffusion') of CO through the diffusion layer (Fig. 9a). In this case, CO diffusion can still be described by a one-dimensional (1D) diffusion transport to a planar Pt surface. On the other hand, the current density, normalized to the active Pt surface area, increases steadily with decreasing Pt coverage, reflecting increasing contributions from spherical diffusion close to the individual nanostructures (Fig. 9b). While qualitatively, the characteristics of the adsorption/reaction kinetics are independent of the transport conditions, the absolute rates of CO adsorption and oxidation, normalized to the Pt coverage, considerably increase with decreasing Pt coverage on glassy carbon electrodes. This behaviour was ascribed to a progressive transition from 1D planar diffusion (concentration gradients planar to the surface-extended Pt surface) to 3D hemispherical diffusion (nanostructured surfaces) [74]. For supported Pt particles, the transition from spherical to planar diffusion is associated to a decrease of the active area. In our opinion, the increase of the ORR activity going from planar to spherical is mainly due to the decrease of the active area.

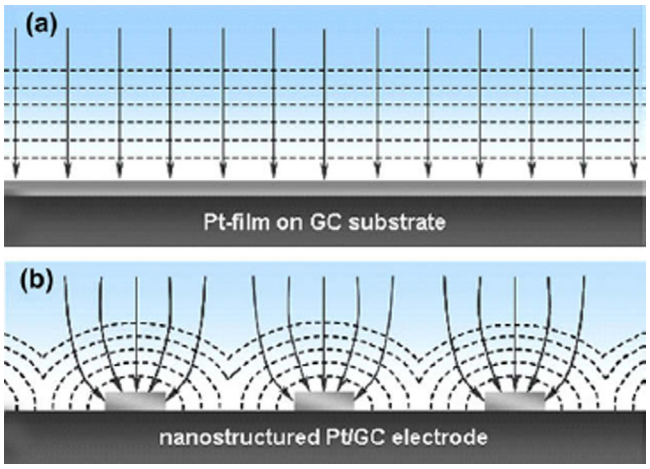

Fig. 9. Schematic description of the diffusion field during a mass transport limited reaction (CO bulk oxidation) over a Pt film electrode (purely vertical diffusion) (a), and a nanostructured Pt/GC electrode (contributions from spherical diffusion close to the nanostructures) (b). Dotted lines: lines of constant CO concentration. Reproduced from Ref. [73], copyright 2010, with permission from Elsevier.

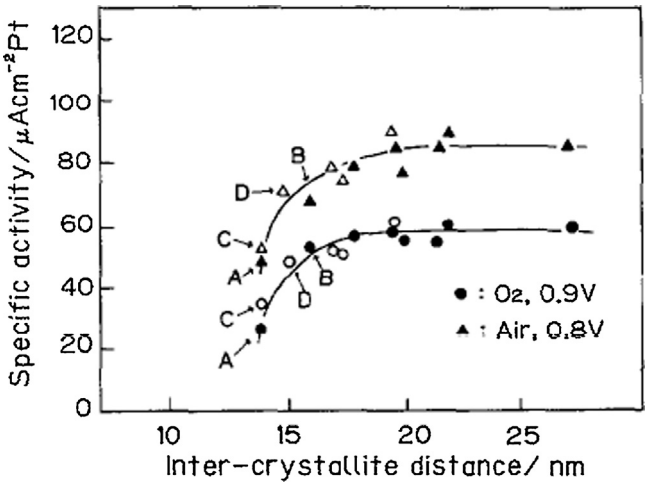

Fig. 10. Specific activity of dispersed platinum crytallites for oxygen reduction at 190 °C in 100% H_3PO_4 as a function of inter-crystallite distance of platinum on the surface of various carbon blacks and various amounts of Pt loading. (●, o) O_2, 0.9 V *vs.* RHE; (▲, Δ) air, 0.8 V *vs.* RHE. (●,▲) Pt supported on different carbon blacks at fixed Pt loading, 10 wt%; (o, Δ) different Pt loadings supported on the same carbon black. A, B: Pt supported on carbons of low surface area less than 100 $m^2 g^{-1}$; C, D: Pt loading 30 and 40 wt%. Reproduced from Ref. [62], copyright 1989, with permission from Elsevier.

The influence of Pt particle size (range from 1.5 to 5 nm) and interparticle distance (range from 12 to 28 nm) on the ORR was investigated by Watanabe et al. [62] in both hot phosphoric acid and sulphuric acid. As shown in Fig. 10, when the inter-particle distance is greater than ~18 nm in pure oxygen and ~20 nm in air, respectively, the specific activity is nearly constant, also for catalysts with low particle size, but when the inter-particle distance is less than 20 (air) or 18 (O_2) nm, the ORR activity decreases with decreasing x_i, independent of the type of carbon support and particle size. They concluded that the catalytic activity doesn't depend on the particle size, but is dependent on the inter-particle distance. More recently, Joo et al. [64], plotting the specific activity for the ORR of Pt supported on ordered mesoporous carbon against the inter-crystallite distance, observed that the specific activity gradually decreases with decreasing the inter-particle distance below 20 nm, supporting the result of Watanabe. The effect of the x_i/d ratio was successful verified by experimental results on ethanol oxidation on

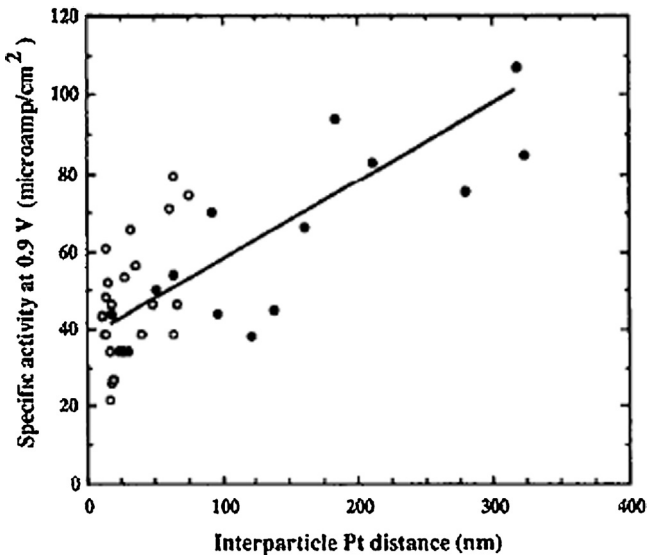

Fig. 11. Specific activity for oxygen reduction at 0.9 V *vs.* RHE as a function of inter-particle Pt distance on carbon support. Solid line indicates the trend of the data. Reproduced from Ref. [66], copyright 1991, with permission from Elsevier.

PtRu/C catalysts with same particle size but different metal loading [65]. The catalytic activity of PtRu/C catalysts decreased with increasing the metal content, that is, with decreasing the x_i/d ratio from 6.7 to 4.2, notwithstanding the concomitant positive effect of the thinner catalyst layer. Giordano et al. [66] investigated the effect x_i of on the ORR activity of Pt/C in a wide range from 20 to 300 nm. As can be seen in Fig. 11, the data showed no clear trend to indicate that a critical inter-particle distance exists, below which a decrease in activity of Pt for oxygen reduction occurs. Instead, the trend of the data suggested that the specific activity decreases monotonically with decreasing the inter-particle distance. In the same way, Kumar and Zou [67] observed that the ORR activity of Pt and PtCo nanoparticle arrays deposited on indium tin oxide (ITO), having the same particle size (4.0 nm) and various inter-particle distances (40, 60, and 80 nm), increases with increasing x_i. Gamez et al. [36] and Watanabe et al. [68], instead, observed no x_i effect on the oxygen reduction and methanol oxidation of Pt/C, respectively, but in these cases x_i/d was always >5.

Summarizing, according to some authors [62,64,65], a threshold value of x_i (x_i about 20 nm) or x_i/d (x_i/d about 5) exists, below which a negative effect on the activity of supported catalysts is present. On the other hand, some papers [66,67] report that, independently of the value of x_i or x_i/d, the activity of supported catalysts monotonously decreases with decreasing x_i.

3.3. Electrochemical double layer potential drop (Pt oxide reduction peak potential increase) (positive effect on the catalytic activity)

Conversely, some works reported a positive effect of x_i and x_i/d, in particular for very low x_i/d ratios, close to 1 (for $x_i/d = 1$ the particles are in contact, that is, the distance between them is = the sum of their radius, resulting in the formation of a extended layer of Pt particles), on the catalytic activity of supported nanoparticles [69–72]. It was observed that size-selected Pt nanoclusters, deposited at high coverage on a glassy carbon substrate, can attain very high ORR activities, particularly in terms of mass-normalized activity. The Pt cluster coverage, and thus the inter-particle distance, significantly affects the catalytic activity, the closely packed assemblies of Pt clusters approaching the surface activity of bulk Pt [69]. Computational modelling indicated that the potential drop in the

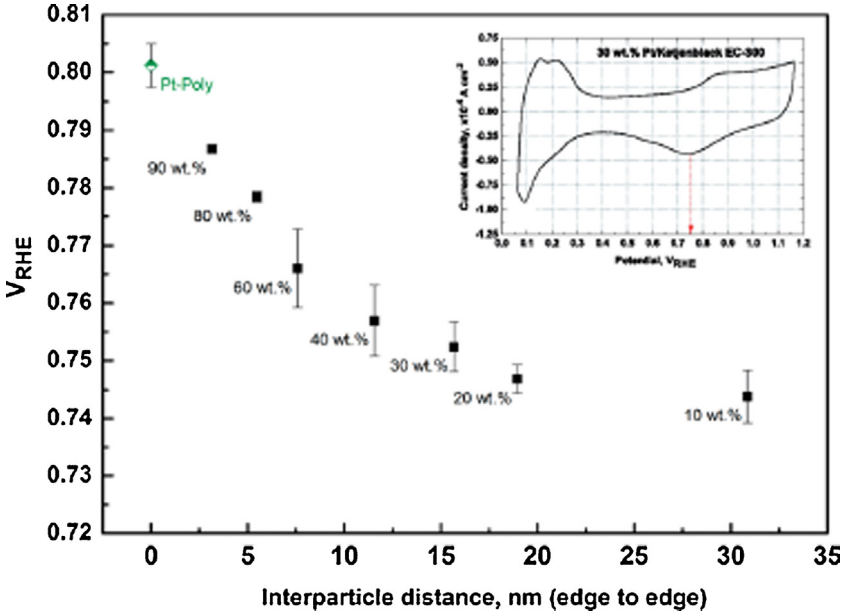

Fig. 12. Pt oxide reduction peak potentials for Pt/Ketjenblack samples with various Pt loading as a function of the calculated interparticle distance (edge to edge). The inset shows the determination of the peak potential using cyclic voltammetry recorded in 0.1 M $HClO_4$ with a sweep rate of 50 mV s^{-1} at room temperature. Reproduced from Ref. [70] with permission from the Royal Society of Chemistry.

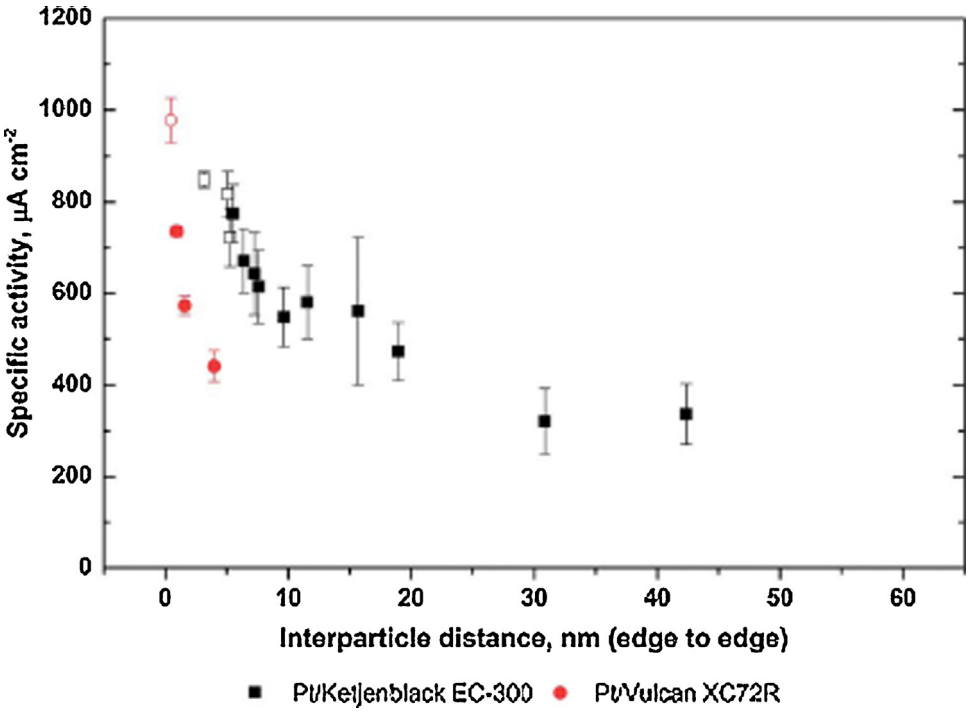

Fig. 13. Surface specific activities (Is) of the model catalysts for ORR as a function of calculated interparticle distance (edge to edge) measured in oxygen saturated 0.1 M $HClO_4$ at 0.9 V_{RHE} and at 20 °C. The open circles and squares represent agglomerated catalyst samples. Under the same conditions Is of polycrystalline Pt is 2 mA $cm^{-2}{}_{Pt}$. Reproduced from Ref. [70] with permission from the Royal Society of Chemistry.

electrochemical double layer (EDL) depends on the inter-particle distance. The model of the particle proximity effect indicated that the EDL of the nanoclusters is a key factor to influence the coverage of an electrode with oxygenated species, the smaller the inter-particle distance, the larger the EDL overlap affecting the potential drop in the compact layer. Such a potential drop should lead to reduced oxide coverage at a given electrode potential. Speder et al. [70] investigated the Pt oxide reduction on Pt/C catalysts: in Fig. 12 it can be seen the dependence of the Pt oxide reduction peak position of Pt/C catalysts on the inter-particle distance, using the peak potential of polycrystalline Pt as a reference. The peak potential varies between 0.8 and 0.75 V *vs.* RHE with polycrystalline Pt having the highest peak potential and the 10 wt% Pt/C sample the lowest, *i.e.*, the peak potential increases with decreasing the inter-particle distance. A correlation of the shift of platinum oxide reduction peak at higher potentials with a weaker adsorption of oxygen-containing species, and, as a consequence, with an increase of the ORR activity of Pt films, was observed by Tammeveski et al. [75].

A strong correlation between the ORR specific activity of Pt/C catalysts with different inter-particle distances and carbon supports and the inter-particle distance was observed by Speder et al. [70] (Fig. 13). As can be seen in Fig. 13, the ORR activity increases with decreasing inter-particle distance. Analogously, Fabbri et al. [71] reported that the transition from dispersed nanoparticles to extended layers lead to a shift of the platinum oxide reduction peak to more positive potentials, resulting in a decrease in the adsorption energy for oxygenated species. The higher specific ORR activity for extended Pt layers was correlated to the lower adsorption energy for oxygenated species, resulting in a lower amount of blocked active sites for the ORR compared to isolated Pt nanoparticles. Moreover, the transition from dispersed Pt nanoparticles to extended layers also influences the Pt selectivity: indeed, at a decreased inter-particle distance, a significant increase in the H_2O_2 production was observed below 0.6 V *vs.* RHE, indicating the significant role of a H_2O_2 desorption-readsorption reaction mechanism during the ORR on Pt nanoparticles. Yang et al. [72] ascribed the decrease of the ORR activity with increasing the inter-particle to the mass transport of H_2O_2. O_2 reduction can occur either through a "direct four-electron" process (parallel pathway) or a "two step" two-electron process (serial pathway). In the "two step" process, H_2O_2 is produced as an intermediate and is further reduced to water. They observed that the amount of H_2O_2 formed on Pt particle arrays increases with increasing the inter-particle distance. This suggests that the "two step" reaction pathway takes place during O_2 reduction. The H_2O_2 produced through the two electron pathway desorbs from the particle surface and diffuses quickly into the bulk solution: the high x_i reduces significantly the probability of H_2O_2 re-adsorption for further reduction to water, decreasing in this way the ORR acticity. Thus, while regarding the effect of x_i on the ORR activity, the works of Fabbri et al. [71] and Yang et al. [72] were in agreement, they reported an opposite effect of the inter-particle distance on the amount of H_2O_2 formed.

Finally, it has to be remarked that x_i is not an independent parameter, but is always depends on d and Me/S.

4. Metal loading (catalyst layer thickness) effect

Supported catalysts, for the same amount of metal loading on the electrode as that of the unsupported black catalysts, give rise to a thicker catalyst layer (CL), due to the large volume of the supporting material. Protons and reactants are transported to Pt particles in electrode CLs. The produced vapor and/or liquid water is then transported outside of the CLs. The diffusivity of reactants in the catalyst layers is controlled by reactant flow rates, the thickness and the porosity of the catalyst layer. Proton transport resistance in the catalyst layers depends on the path length for protons transport, which in turn depends on the CL thickness. The increase of CL thickness results in an increase in proton transport path length and, thus, in an increase in proton transport resistance. Starting from the flooded agglomerate model, Kamarajugadda and Mazumder [76] investigated numerically the effect of the cathode CL structure and composition on the overall performance of a PEMFC: the change of the Pt|C ratio with a fixed Pt loading in the electrode results in a change of the amount of carbon within the agglomerates. Moreover, since the volume fraction of Nafion within the agglomerate has also to be unchanged, change in the amount of carbon must also be accompanied by a change in the amount of Nafion within the catalyst layer. Thus, low values of the Pt|C ratio result in large amounts of carbon, which also results in large amounts of Nafion. As a consequence, low Pt|C ratios give rise to poor PEMFC performances, owing to an increased mass transport resistance to diffusion of gases through the pores,. On the other hand, excessively high values of the Pt|C ratio result in too little Nafion within the cathode, reducing the protonic conductivity of the cathode. A schematic representation of the catalyst layers with the same metal loading is shown in Fig. 14 [77]: for high Pt/C ratios, the reactant can penetrate into the catalyst layer easily (Fig. 14a), while for low Pt/C ratios, the reactant path is more complex and longer (Fig. 14b). For minimizing fuel cell performance losses, due to limitations of the rate of proton diffusion within the CL and the rate of mass transfer of the chemical reactants and products to and from the active sites, the CL must be relatively thin [78]. To minimise the CL thickness, the metal loading in catalysts for fuel cell applications is typically 20 wt% or greater, in contrast to normal industrial supported metal catalysts which are usually under 5 wt%. Regarding the PEMFCs operating with H_2/O_2 or H_2/air, generally the diffusivity of O_2 molecules in the cathode is much lower than that of H_2 molecules in the anode, and, thus, the feasibility of O_2 to reach catalyst particles in the cathode is more important than that of H_2 in the anode. Thus, studies have been devoted to evaluate the effect of cathode catalyst layer thickness on the ORR [67–69]. Ticianelli et al. [79] fabricated PEMFC cathodes using Pt/C catalysts with Pt loadings of 10, 20, and 40 wt%, at a fixed Pt loading (0.4 mg cm^{-2}) in the electrode. The thickness of the CL was 100, 50, and 25 μm for electrodes with 10, 20, and 40 wt% Pt/C, respectively. Fuel cell tests clearly indicated that decreasing the CL thickness an improvement in PEMFC performance in all three current density regions (activation, ohmic, and mass transport) takes place. The cell with 40 wt% Pt/C on the cathode side, however, showed only a slight improvement of performance compared to the cell with 20 wt% Pt/C, due to the larger particle size in the 40 wt% Pt/C than in the 20 and 10 wt% Pt/C, resulting in a smaller Pt surface area, and counteracting the positive effect of thinner layer. Yang et al. [80] prepared four membrane electrode assemblies (MEAs) with different catalysts layers, that is, (i) a catalyst layer with 40% Pt/C (particle size 2.8 nm) between the polymer electrolyte membrane (PEM) and the gas diffusion layer (GDL), (ii) a catalyst layer with 40% Pt/C plus a thin catalyst layer with 80% Pt/C (particle size 4.9 nm) at the interface between the 40% Pt/C layer and PEM, (iii) a catalyst layer with 40% Pt/C plus a thin catalyst layer with 80% Pt/C at the interface between the 40% Pt/C layer and GDL, and (iv) a catalyst layer consisting of a homogeneous mixture of 40% Pt/C and 80% Pt/C between PEM and GDL. The total amount of Pt loading was the same in all the MEAs. The replacement of 20–40 wt% of 40% Pt/C with 80% Pt/C causes a reduction of the content of carbon and, as a consequence, of CL thickness. The lower CL thickness results in a lower proton transport resistance in catalyst layers and a higher efficiency for the O_2 molecules to reach cathode Pt sites, particularly when the fuel cell is operating at a high current densities. On the other hand, the replacement of part of 40% Pt/C with 80% Pt/C causes a loss of Pt particles surface area and thus of Pt catalytic activity. As the negative effect of activity loss on cell performance is lower than the positive effect of the reduction of proton transport resistance and mass transport, all the MEAs with 40% + 80% Pt/C better performed than the 40% Pt/C MEA. Moreover, the effect of the catalyst layer structure on cell performance depends on O_2 flow rate. Indeed, comparing the MEAs with same amount of 40% and 80% Pt/C catalysts, at a low H_2/O_2 flow rate the MEA with the 80% Pt/C near GDL better performed than the MEA with the 80% Pt/C layer near PEM, while at a high H_2/O_2 flow rate an opposite result was observed. Analogously, Mamlouk et al. [81] observed that the effect of the CL thickness on the performance of an alkaline membrane fuel cell depends on cell operation either with O_2 or with air. Fig. 15 shows the effect of cathode catalyst layer thickness on fuel cell performance at 60 °C at a fixed Pt loading using 30, 40, and 60% Pt/C catalysts. The increase of the Pt/C ratio lead to both a thinner catalyst layer and a lower surface area by the increase of the particle size. Under O_2 operation, the reduction of the Pt/C ratio from 60 to 40% increased cell performance, but a further reduction of the Pt/C

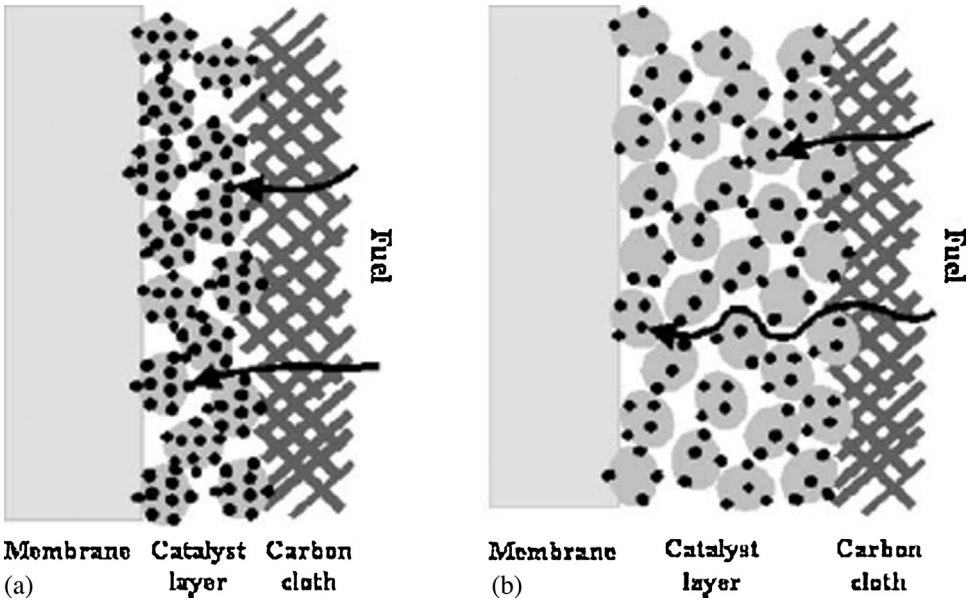

Fig. 14. Schematic representation of catalyst layers with the same metal loading. (a) at the high metal ratio catalyst, the reactant could penetrate to the catalyst layer easily and (b) at the low metal ratio catalyst, the reactant paths are more complex and longer than those of the case (a). Reproduced from Ref. [77], copyright 2004, with permission from Elsevier.

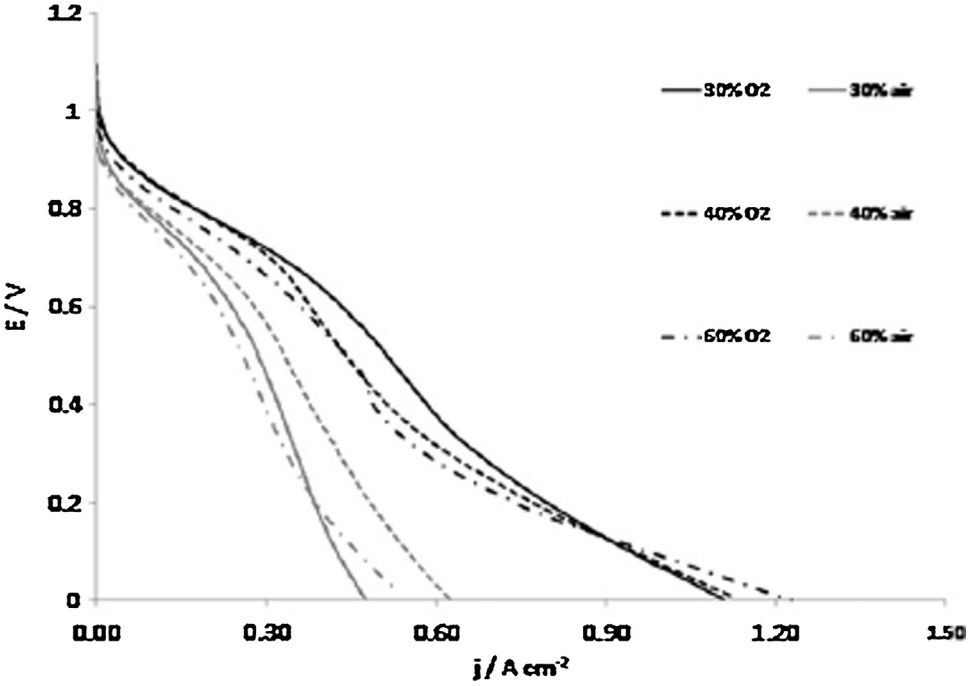

Fig. 15. Effect of cathode catalyst layer thickness on fuel cell performance at 60 °C with 0.4 mg_{Pt} cm^{-2} 30, 40 and 60% Pt/C and 30% ionomer content, gases at atmospheric pressure and a 30% Pt/C anode. Reproduced from Ref. [81], copyright 2011, with permission from Elsevier.

ratio to 30% gave rise to only a little improvement. This behaviour was directly correlated to the order of electrochemically active surface area. However under air operation, 40% Pt/C showed the best performance followed by 30% and then 60% Pt/C. In this case with a lower oxygen concentration, the positive effect of thinner layer using 40% Pt/C prevailed on the negative effect of the lower surface area with respect to 30% Pt/C. All these works highlight the close relationship between metal loading on the carbon, particle size and catalyst layer thickness and their effect on fuel cell performance.

Regarding the effect of the anode CL on the performance of direct methanol fuel cells (DMFCs), Lee et al. [77] observed that in the high current region, the performance of the cell with 80 wt% PtRu/C catalyst in the anode CL, that is, with the lowest CL thickness, was superior to that of the cells with 40 and 60 wt% PtRu/C catalysts, as shown in Fig. 16.

To evaluate the net effect of catalyst layer thickness, a way to prepare a catalyst layer with different thickness without changes in catalyst particle size and inter-particle distance was proposed, consisting in the addition of carbon black particles to the supported catalyst. Suzuki et al. [82] determined the CL thickness (in the range 5–14 μm), maintaining the other parameters constant, by blending Pt/C and uncatalized carbon black. Then, the effect of catalyst

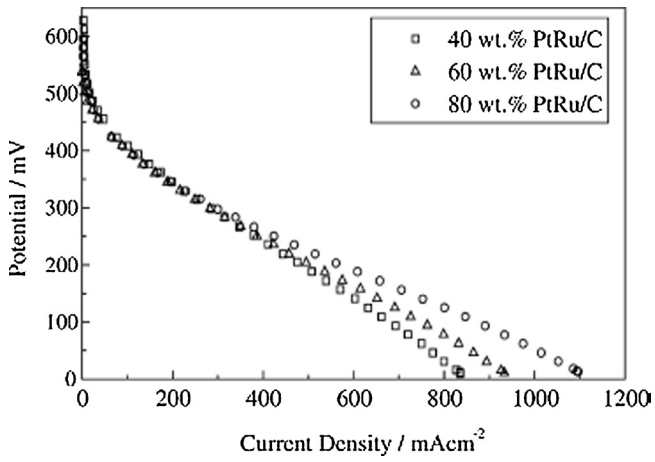

Fig. 16. Polarization curves for DMFC MEAs with a constant amount of metal (5 mg cm^{-2}) but different catalyst layer thicknesses. Reproduced from Ref. [77], copyright 2004, with permission from Elsevier.

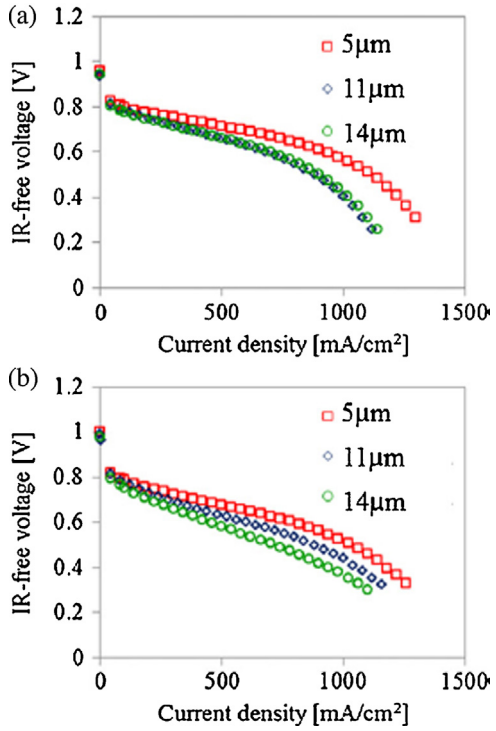

Fig. 17. Cell performances of the thickness-parameter CLs supplying H_2/Air. RH conditions of the cells are (a) 40% RH and (b) 90% RH. Reproduced from Ref. [82], copyright 2013, with permission from Elsevier.

layer thickness on PEMFC performance was evaluated. The properties of the Pt/C catalyst, such as the ECSA, were independent of CL thickness, so the difference in the performance of PEMFCs with various catalyst layers was ascribed to differences in mass transport. Polarization curves of H_2/air PEMFCs with the same Pt/C 20 wt% catalyst but different CL thickness, at a fixed Pt loading, are shown in Fig. 17a (40% RH) and b (90% RH). The thinnest CL (5 μm) showed the best performance, due to the highest mass transport. For low RH (Fig. 17a), the difference in the PEMFC performance for 5 μm and 11 μm CL thickness is larger than the corresponding one for high RH (Fig. 17b): in low RH conditions, proton transport in the CLs is poorer than in high RH conditions due to lower proton conductivity, thus the effect of CL thickness is more pronounced. However, the dilution of carbon supported Pt by uncatalised carbon black addition is not irrelevant on the catalyst performance: indeed, Lee et al. [83] observed a positive effect of carbon black dilution on the activity of Pt/C. MA increased with increasing carbon content in the CL from 50 to 70 wt%. This result suggests that the transport resistance for reactant gas, that is, the O_2 diffusion resistance at the surface of the catalysts and through the binder in the CL, decreased with increasing Pt dispersion. In the case of air, MA attained a maximum for a total carbon content of 70 wt% at all RH values. Then, for a carbon content of 80 wt% in the CL, MA slightly decreased in comparison with the CL with 70 wt% of carbon, as the increase of the proton transport resistance through the binder was prevalent on the positive effect of carbon dilution on the O_2 transport resistance. In the case of O_2, the effect of CL thickness was less important, and was evident only at low humidification (53% and 30% RH).

5. Effect of the link between Me/*S*, *d* and x_i on the catalytic activity

Generally, metal particles size increases with increasing the Me/*S* ratio [84–89], thus, at a fixed metal loading in the catalyst layer, the use of catalysts with high metal Me/*S* ratio results in a decrease the thickness of the catalyst layer and, on the other hand, in an increases metal particle size. As a consequence, the positive effect of the proton transport resistance decrease and reactant mass transport increase in the catalyst layer is counterbalanced by the negative effect of the catalyst mass activity decrease. On the other hand, using appropriate synthesis methods the same particle size can be obtained for different Me/*S* ratios [84,90,91]. In this case, however, the use of catalysts with high Me/*S* in the catalyst layer decreases the inter-particle distance, which also affects the catalytic activity. Indeed, starting from the following relation [92,93]:

$$\frac{Me}{S} = \frac{y}{(1-y)} = n_p m_p \tag{2}$$

where *y* is the metal fraction in the catalyst, n_p is the particle number per unit mass of carbon and m_p is the particle mass. m_p can be expressed as:

$$m_p = \frac{NpM_w}{N_A} \tag{3}$$

where *Np* is the number of atoms per metal particle, M_w is the atomic weight of the metal and N_A is the Avogadro's number. Considering that the particle diameter is defined as the diameter of a sphere (*d*) with a volume equal to N_p times the volume occupied by an atom in the unit cell [92,93], it has for metals or alloys with fcc crystal structure such as Pt and Pt-based alloys:

$$d = a\left(\frac{6N_p}{4\pi}\right)^{1/3} \tag{4}$$

where *a* is the lattice parameter of the metal or the alloy, and that the relation between the inter-particle distance x_i and n_p, based on the close pack arrangement of metal particles, is:

$$x_i = \left(\frac{SSA_S}{n_p}\right)^{1/2} \tag{5}$$

where SSA_S is the specific surface area of the support. From Eqs. (2–5) it results:

$$\frac{Me}{S} = \frac{4\pi SSA_S d^3 M_w}{N_A\left(6x_i^2 a^3\right)} \tag{6}$$

Thus, from Eq. (6) it can be inferred that an increase of Me/*S* gives rise to an increase of *d* and/or a decrease of x_i. Clearly, for a constant value of *d*, x_i decreases with increasing metal loading. The

relationship between the density of the metal catalyst (ρ) and the lattice parameter a is:

$$\rho = \frac{zM_w}{\left(N_A a^3\right)} \tag{7}$$

where z is the number of atoms per unit cell.

Based on Eqs. (2–7), the general relationship between particle size, inter-particle distance and metal loading of carbon supported catalysts can be expressed as:

$$\frac{y}{(1-y)} = \frac{4\pi\rho d^3 \mathrm{SSA_S}}{\left(6zx_i^2\right)} \tag{8}$$

For Pt particles it results [62]:

$$x_i = \left(\frac{1}{3}\right)\left[\frac{3^{0.5}\pi\rho d^3 \mathrm{SSA_S}\,(1-y)}{y}\right]^{0.5} \tag{9}$$

As reported in Section 3, the x_i/d ratio seems to be a better parameter than x_i affecting the catalytic activity of supported catalysts. From Eq. (9) it follows that the square of x_i/d linearly increases with increasing d as:

$$\left(\frac{x_i}{d}\right)^2 = \left(\frac{1}{9}\right)\left[\frac{3^{0.5}\pi\rho \mathrm{SSA_S}\,(1-y)}{y}\right] d \tag{10}$$

The optimum Pt particle size of supported catalysts for a successful use in fuel cells is in the range 2–4 nm. As reported in Section 3, when the x_i/d ratio is lower than 5, an inter-particle distance effect takes place, regarding which two different models were proposed. According to the Model 1 (shielding effect), for $x_i/d < 5$ a negative inter-particle distance effect is present, decreasing the activity of the catalyst. From Eq. (10) it follows that for a given value of x_i/d the particle size depends on the metal loading. Fig. 18a shows the dependence of d on Pt content in the catalyst for carbon supports with different surface area, at a fixed x_i/d value of 5. The solid line represents the value of d_{opt} = 3 nm, that is, an optimal value of particle size. As can be seen in Fig. 18a, d monotonously increases with increasing metal content in the catalyst. For high metal loadings, the positive effect of a thinner catalyst layer is concomitant to a decrease of the effective catalyst surface area due to an increase of d and/or a decrease of x_i/d compared to their optimum values, with in turns gives rise to a decrease in the catalytic activity. The maximum metal loading $(\mathrm{Me}/S)_{max}$, at which the optimum values of d (3 nm) and x_i/d (>5) can be obtained, depends on support surface area: $(\mathrm{Me}/S)_{max}$ increases from *ca.* 30 wt% to *ca.* 40 wt% to >50 wt% going from Vulcan carbon (SSA = 254 $m^2\,g^{-1}$ [94]) to carbon nanotubes (CNT) (surface area near 400 $m^2\,g^{-1}$ [94]) to graphene (GN) (surface area *ca.* 800 $m^2\,g^{-1}$ [95,96]). According to the Model 2 (electrochemical double layer potential drop), instead, for $x_i/d < 5$ a positive inter-particle distance effect is present, increasing the activity of the catalyst. Fig. 18b shows the dependence of d on Pt content in the catalyst for carbon supports with different surface area, at a fixed x_i/d value of 1, an optimal condition, corresponding to an extended Pt surface. As expected, the optimal value of particle size (3 nm) for $x_i/d = 1$ is attained at very high metal loadings.

Some doubts regarding the exact effect of particle size and inter-particle distance on the specific activity of supported catalysts, evaluated by using catalyst thick layers, as in the case of 'in situ' fuel cell measurements, however, can be aroused by the correlation between d, x_i and Me/S. In a reasonable approximation, based on experimental trends, we can assume the specific activity for the ORR proportional to ln d for $d < 6$ nm and independent of d for $d \geq 6$ nm, proportional to ln x_i/d for $x_i/d \leq 5$ nm and independent of x_i/d for $x_i/d > 5$, and directly proportional to Me/S. The effect of Me/S on the SA accounts for the proton and reactant transport rate, and a linear dependence of SA on Me/S can be assumed. On these bases,

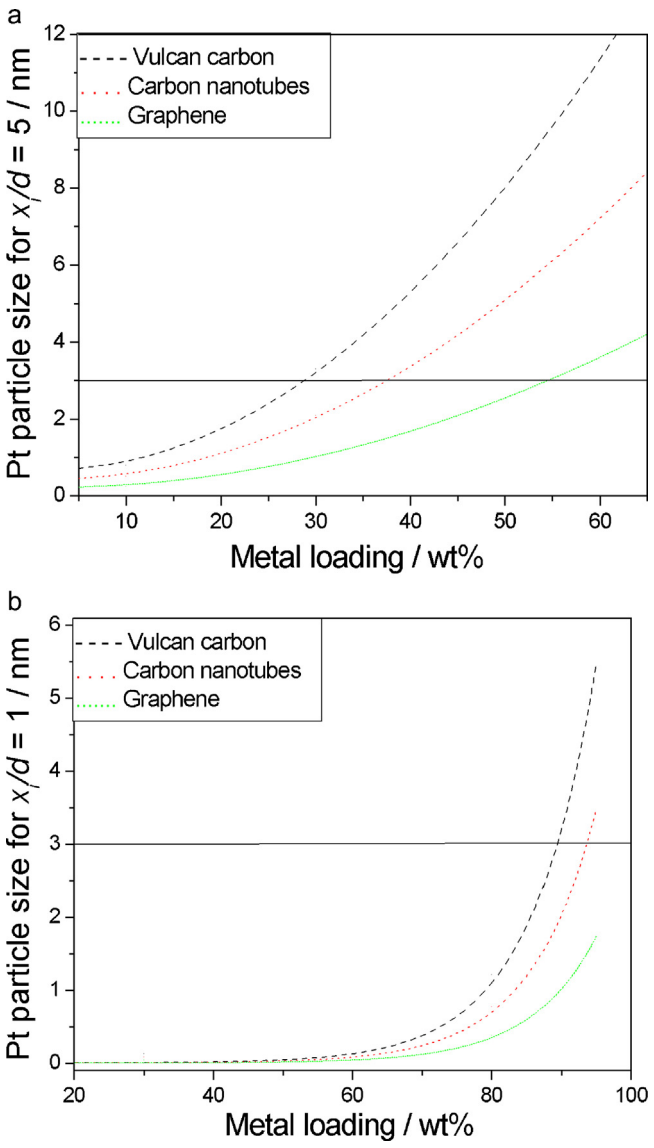

Fig. 18. Dependence of Pt particle size on metal content in the catalyst for (a) for $x_i/d = 5$ and (b) $x_i/d = 1$. The solid line represents the value of d_{opt} = 3 nm.

and assuming the effects of d, x_i/d and Me/S on the catalytic activity independent of each other, the relation between SA, d, x_i/d and Me/S can be expressed as:

$$\mathrm{SA} = \mathrm{SA}_o + (\mathrm{SA}_m - \mathrm{SA}_o)\left[\frac{k_1\,(\ln d - \ln d_o)}{(\ln d_m - \ln d_o)} \pm \frac{k_2\left(\ln x_i/d - \ln x_{io}/d\right)}{\left(\ln\left(x_i/d\right)_m - \ln\left(x_i/d\right)_o\right)} + \frac{k_3\left(\mathrm{Me}/S - \left(\mathrm{Me}/S\right)_o\right)}{\left(\left(\mathrm{Me}/S\right)_m - \left(\mathrm{Me}/S\right)_o\right)}\right] \tag{11}$$

where SA_o is the minimum value of the specific activity of the catalyst in the presence of a negative effect of d, that is, for d_o = 1 nm (very small particles), a negative/positive effect of x_i/d ($(x_i/d)_o = 1$, a very short inter-particle distance to particle size ratio), and a negative effect of Me/S ($(\mathrm{Me}/S)_o$, the lowest metal loading (*ca.* 0.05, resulting in a very thick CL)), and SA_m is the maximum value of the specific activity obtained for $d_m \geq 6$ nm, $(x_i/d)_m \geq 5$, and $(\mathrm{Me}/S)_m$ (the highest metal loading (*ca.* 0.9, resulting in a very thin CL)), and k_1, k_2 and k_3 are constants, with $k_1 + k_2 + k_3 = 1$. d_m = 6 nm for

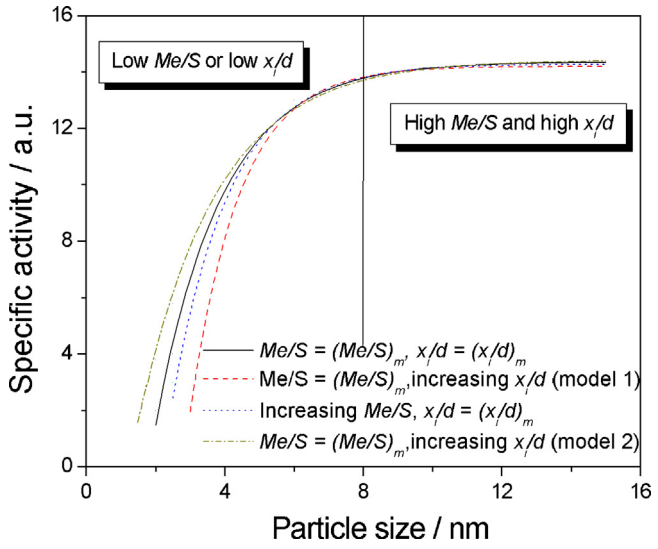

Fig. 19. Qualitative dependence of the ORR specific activity on particle size in different conditions. Solid line: theoretical Me/*S* and x_i/d optimum condition, *i.e.*, absence of other effect than particle size effect; dashed line: effect of x_i/d increase (according to Model 1) on SA/*d* plot at a high (optimum) Me/*S* value; dotted line: effect of Me/*S* increase on SA/*d* plot at a high (optimum) x_i /*d* value; dashed dotted line: effect of x_i/d increase (according to Model 2) on SA/*d* plot at a high (optimum) Me/*S* value.

$d \leq 6$ nm, $d_m = d$ for $d > 6$ nm; $(x_i/d)_m = 5$ for $x_i/d \leq 5$, $(x_i/d)_m = x_i/d$ for $x_i/d > 5$. As previously reported, the control of particle size is usually achieved by changing metal loading in the catalyst. The use of activity data obtained from catalysts with a different metal loading for the evaluation of the particle size effect could not be correct considering the effect of Me/*C* on the electrochemically active surface area. Also the use of supported catalysts with the same metal loading, however, presents some uncertainty. Indeed, at fixed Me/*S*, the inter-particle distance, which also affects the catalytic activity, depends on particle size. On the other hand the inter-particle distance depends on particle size and metal content in the catalyst. The change of x_i occurs together with a change of *d* and/or Me/*S*, thus the true effect of the inter-particle distance on the catalytic activity is difficult to be determined. Considering that, below certain values of *d* and x_i, the catalytic activity decrease with decreasing particle size and inter-particle distance, the decrease of Me/*S* and/or x_i (for the size) also affect the activity of the catalyst. Qualitative specific activity/particle size plots are shown in Fig. 19. As the effect of x_i/d on SA/*d* plot has to be shown for a fixed value of Me/*S*, we chose Me/S_m. Indeed, at small particle sizes (in the range 2–4 nm), a low x_i/d value, at which the difference between Model 1 and 2 is important, can be obtained only for high Me/*S* values. As it is very difficult to evaluate the relative contribute of *d, x*, and Me/*S* on the ORR activity, that is, the values of the parameter k_1, k_2 *and* k_3, the curves in Fig. 19 are absolutely qualitative. The aim of Fig. 19 is to show the effect of x_i/d and Me/*S* on SA/*d* plot. At small particle sizes both the decrease of Me/*S* at a fixed high x_i/d (absence of inter-particle distance effects) (dotted line) and the decrease of x_i/d, at a fixed high Me/*S*, (thin CL thickness) (dashed and dashed-dotted lines), have an additional negative/positive effect on the catalytic activity compared to the activity of an ideal not realizable catalyst with fixed Me/*S* and x_i (solid line). Thus, the effect of particle size could be over/underestimated.

5. Conclusions

Some physical characteristics of supported fuel cell catalysts affect their catalytic activity. Metal particle size and inter-particle distance are key parameters influencing the catalytic activity of supported catalysts and, hence, fuel cell performance. Moreover, metal loading, that is, the amount of metal present on the support, affecting the thickness of the fuel cell catalyst layer, also influence cell performance. There is a broad consensus on the effect of particle size on the mass activity, which has practical implications, because the cost of the electrode depends on the amount of precious metal used, while the specific activity is more useful to compare the intrinsic activity of the different catalysts: the dependence of the MA of platinum on particle size goes through a maximum, with an optimum *d* value of about 3 nm for oxygen reduction and about 2 nm for methanol oxidation. The Pt specific activity for the ORR, however, shows a different behaviour with respect to the SA for the MOR. Indeed, in the case of the ORR, except few works, which report no effect of particle size for small size ($d \leq 5$ nm), the SA always increases with increasing particle size, up to reach the level of the bulk or polycrystalline surface; the MOR activity, instead, can either increase or decrease with increasing particle size. In our opinion, the most realistic effect of particle size on the SA of methanol oxidation is represented by a volcano curve with a maximum at about 2.5 nm. The different effect of the particle size on oxygen reduction and alcohol oxidation has to be ascribed to the different effect of OH adsorption on these reactions. In the former case the effect of OH adsorption is only negative, reducing the active sites required for the adsorption of O_2. In the latter case, instead, in addition to the negative effect, due to the blocking the active sites required for the adsorption of CH_3OH, the adsorbed OH also acts as a promoter of the oxidation of adsorbed alcohol oxidation intermediated.

In the case of the inter-particle distance, two model have been proposed, both supported by experimental data: Model 1 is based on the diffusion and/or the shielding effect of the inter-particle distance. When metal particles are close together within some critical region, there is a mutual influence on the diffusion, or some other parameter, such that the whole area is not available. In other words, with the decrease of x_i or x_i/d, the diffusion characteristics changes from the spherical diffusion of isolated Pt nanoparticles to an about planar diffusion typical of Pt films. On the other hand, Model 2 is based on the dependence of the potential drop in the electrochemical double layer on the inter-particle distance. This model indicated that the EDL of the nanoclusters is a key factor to influence the coverage of an electrode with oxygenated species, the smaller the inter-particle distance, the larger the EDL overlap affecting the potential drop in the compact layer. Such a potential drop should lead to reduced oxide coverage at a given electrode potential. Whereas Model 1 predicts a decrease of the catalytic activity with decreasing the inter-particle distance, according to Model 2, the catalytic activity increases with decreasing x_i. It seems that the positive effect on the ORR activity appears especially for very low x_i/d (close to 1), for which overlapping of nanoparticle EDLs is possible. The conflicting results on the effect of inter-particle distance on the ORR activity could be the result of the preparation method used in these studies. By preparation techniques such as impregnation or precipitation methods it is really hard to change individual parameters, *i.e.*, an increase in the metal weight loading (decreasing inter-particle distance) results also in an increase of the Pt particle size. Generally, in the case of works explained by Model 1 Pt particle size is not constant, while in the case of works supporting Model 2 no Pt particle size increase occurs with increasing Pt/C ratio. Thus, Model 2 would seem more reliable. Further studies are needed to clearly determine the effect of x_i on the ORR. The decrease of the activity for ethanol oxidation of PtRu/C catalysts with decreasing the *xi* /d ratio was explained by the Model 1 [65]. However, the Model 2 can be invoked also to explain the decrease of the EOR activity with decreasing x_i by the reduction of the amount of adsorbed OH, acting as a promoter of the oxidation of adsorbed alcohol oxidation intermediated. Interestingly, in the case of the ORR, Models 1 and 2 were proposed to explain diver-

gent experimental results, whereas, in the case of the EOR, the same experimental result can be explained by both Models.

To achieve high proton conductivity and mass transport rate, particularly for fuel cell operating with air, the use of catalysts with a high metal loading on the support is necessary to reduce the catalyst layer thickness. A high metal loading, however, can be obtained only simultaneously with a particle size increase and/or inter-particle distance decrease, that is, a high Me/*S* is often associate to a decrease of the catalytic activity. Theoretical evaluations on the effect of the link between Me/*S*, *d* and x_i on the catalytic activity indicated that, for Model 1 the optimum characteristic of the catalyst ($d = 3$, $x_i/d > 5$) can be obtained for a maximum metal loading of 30, 40, and 50 wt% for carbon black, carbon nanotubes and graphene, respectively. On the other hand, for Model 2 the optimum characteristic of the catalyst ($d = 3$, $x_i/d = 1$) are attained only for very high metal loadings.

Some doubts regarding the effect of size and x_i on the activity of supported catalysts evaluated by using catalyst thick layers, as in the case of 'in situ' fuel cell measurements, however, can be aroused by the correlation between *d*, x_i, and Me/*S*. The use of activity data obtained from catalysts with a different metal loading could not be correct considering the effect of Me/*S* on the proton and mass transport. Also the use of catalysts with the same metal loading, however, presents some uncertainty. Indeed, at fixed Me/*S*, the particle size and the inter-particle distance are linked, according to Eq. (10). At a fixed Me/*S*, the change of x_i occurs together with a change of *d*, thus the true effect of the particle size and the inter-particle distance on the catalytic activity is difficult to be determined. On these bases, better understanding is still required regarding the effect that particle size and inter-article distance may play in chemical reactivity.

Summarizing, for a high cell performance it is necessary to attain a good compromise between Me/*S*, *d*, and x_i, which can depend on the use of the catalyst in the fuel cell. For example, a thinner layer, that is, a high Me/*S*, is preferred for the cathode, particularly when the cell operates in air, resulting in a penalization of the catalytic activity due to larger *d* or shorter x_i values than their optimum values. For a PEMFC anode, instead, the thickness of the catalyst layer is less important, thus an appropriate Me/*S* ratio can be chosen, which allows to obtain the optimal value of particle size and inter-particle distance.

References

[1] Y. Wang, K.S. Chen, J. Mishler, S.C. Cho, X. Cordobes, Appl. Energy 88 (2011) 981–1007.
[2] S.P.S. Badwal, S. Giddey, A. Kulkarni, J. Goel, S. Basu, Appl. Energy 145 (2015) 80–103.
[3] S.K. Kamarudin, N. Hashim, Renew. Sustain. Energy Rev. 16 (2012) 2494–2515.
[4] E. Antolini, Mater. Chem. Phys. 78 (2003) 563–573.
[5] O.A. Petrii, J. Solid State Electrochem. 12 (2008) 609–642.
[6] E. Antolini, E.R. Gonzalez, Catal. Today 160 (2011) 28–38.
[7] A. Serov, C. Kwak, Appl. Catal. B Environ. 90 (2009) 313–320.
[8] A. Brouzgou, S.Q. Song, P. Tsiakaras, Appl. Catal. B Environ. 127 (2012) 371–388.
[9] S. Gottesfeld, T.A. Zawodzinski, Polymer electrolyte fuel cells, in: R.C. Alkire, H. Gerischer, D.M. Kolb, C.W. Tobias (Eds.), Advances in Electrochemical Science and Engineering, 1st edition, Wiley-VCH, Weinheim, 1997, pp. 195–210 (Chapter 5).
[10] Z. Liu, L. Ma, J. Zhang, K. Hongsirikarn, J.G. Goodwin, Catal. Rev. Sci. Eng. 55 (2013) 255–288.
[11] J. Greeley, I.E.L. Stephens, A.S. Bondarenko, T.P. Johansson, H.A. Hansen, T.F. Jaramillo, J. Rossmeisl, I. Chorkendorf, J.K. Nørskov, Nat. Chem. 1 (2009) 552–556.
[12] M. Li, Y. Lei, N. Sheng, T. Ohtsuka, J. Power Sources 294 (2015) 420–429.
[13] H. Yano, M. Kataoka, H. Yamashita, H. Uchida, M. Watanabe, Langmuir 23 (2007) 6438–6445.
[14] M. Watanabe, D.A. Tryk, M. Wakisaka, H. Yano, H. Uchida, Electrochim. Acta 84 (2012) 187–201.
[15] L. Ou, Comput. Theor. Chem. 1048 (2014) 69–76.
[16] M.K. Jeon, P.J. McGinn, Electrochim. Acta 64 (2012) 147–153.
[17] L. Liu, G. Samjeske, S.L. Nagamatsu, O. Sekizawa, K. Nagasawa, S. Takao, Y. Imaizumi, T. Yamamoto, T. Uruga, Y. Iwasawa, Topics Catal. 57 (2014) 595–606.
[18] N. Jung, D.Y. Chung, J. Ryu, S.J. Yoo, Y.E. Sung, Nano Today 9 (2014) 433–456.
[19] Y.H. Bing, H.S. Liu, L. Zhang, D. Ghosh, J.J. Zhang, Chem. Soc. Rev. 39 (2010) 2184–2202.
[20] F. Maillard, E.R. Savinova, P.A. Simonov, V.I. Zaikovskii, U. Stimming, J. Phys. Chem. B 108 (2004) 17893–17904.
[21] F.J. Perez-Alonso, D.N. McCarthy, A. Nierhoff, P. Hernandez-Fernandez, C. Strebel, I.E.L. Stephens, J.H. Nielsen, I. Chorkendorff, Angew. Chem. Int. Ed. 51 (2012) 4641–4643.
[22] S. Park, Y. Xie, M.J. Weaver, Langmuir 18 (2002) 5792–5798.
[23] K. Kinoshita, J. Electrochem. Soc. 137 (1990) 845–848.
[24] J. Perez, E.R. Gonzalez, E.A. Ticianelli, Electrochim. Acta 44 (1998) 1329–1339.
[25] J. Greeley, J. Rossmeisl, A. Hellman, J.K. Norskov, Z. Phys, Chem. 221 (2007) 1209–1220.
[26] S. Mukerjee, J. McBreen, J. Electroanal. Chem. 448 (1998) 163–171.
[27] Y. Takasu, N. Ohashi, X.G. Zhang, Y. Murakami, H. Minagawa, S. Sato, K. Yahikozawa, Electrochim. Acta 41 (1996) 2595–2600.
[28] K.J.J. Mayrhofer, B.B. Blizanac, M. Arenz, V.R. Stamenkovic, P.N. Ross, N.M. Markovic, J. Phys. Chem. B 109 (2005) 14433–14440.
[29] L.S. Park, K.W. Park, J.H. Choi, C.R. Park, Y.E. Sung, Carbon 45 (2007) 28–33.
[30] H. Yano, J. Inukai, H. Uchida, M. Watanabe, P.K. Babu, T. Kobayashi, J.H. Chung, E. Oldfield, A. Wieckowski, Phys. Chem. Chem. Phys. 8 (2006) 4932–4939.
[31] M. Nesselberger, S. Ashton, J.C. Meier, I. Katsounaros, K.J.J. Mayrhofer, M. Arenz, J. Am. Chem. Soc. 133 (2011) 17428–17433.
[32] W. Sheng, S. Chen, E. Vescovo, Y. Shao-Horn, J. Electrochem. Soc. 159 (2012) B96–B103.
[33] N.M. Marković, R.R. Adžić, B.D. Cahan, E.B. Yeager, J. Electroanal. Chem. 377 (1994) 249–259.
[34] N.M. Markovic, H.A. Gasteiger, P.N. Ross, J. Phys. Chem. 99 (1995) 3411–3415.
[35] A. Kabbabi, F. Gloaguen, F. Andolfatto, R. Durand, J. Electroanal. Chem. 373 (1994) 251–254.
[36] A. Gamez, D. Richard, P. Gallezot, F. Gloaguen, R. Faure, R. Durand, Electrochim. Acta 41 (1996) 307–314.
[37] H. Ye, J.A. Crooks, R.M. Crooks, Langmuir 23 (2007) 11901–11906.
[38] A. Sarapuu, A. Kasikov, T. Laaksonen, K. Kontturi, K. Tammeveski, Electrochim. Acta 53 (2008) 5873–5880.
[39] M. Shao, A. Peles, K. Shoemaker, Nano Lett. 11 (2011) 3714–3719.
[40] K.J.J. Mayrhofer, D. Strmcnik, B.B. Blizanac, V. Stamenkovic, M. Arenz, N.M. Markovic, Electrochim. Acta 53 (2008) 3181–3188.
[41] M.L. Sattler, P.N. Ross, Ultramicroscopy 20 (1986) 21–28.
[42] J.T. Hwang, J.S. Chung, Electrochim. Acta 38 (1993) 2715–2723.
[43] F. Maillard, M. Martin, F. Gloaguen, J.M. Léger, Electrochim. Acta 47 (2002) 3431–3440.
[44] K. Jayasayee, J.A.R. Van Veen, T.G. Manivasagam, S. Celebi, E.J.M. Hensen, F.A. de Bruijn, Appl. Catal. B Environ. 111–112 (2012) 515–526.
[45] I. Katsounaros, S. Cherevko, A.R. Zeradjanin, K.J.J. Mayrhofer, Angew. Chem. Int. Ed. 53 (2014) 102–121.
[46] M. Peuckert, T. Yoneda, R.A. Dalla Betta, M. Boudart, J. Electrochem. Soc. 133 (1986) 944–947.
[47] H.A. Gasteiger, S.S. Kocha, B. Sompalli, F.T. Wagner, Appl. Catal. B Environ. 56 (2005) 9–35.
[48] Z. Xu, H. Zhang, H. Zhong, Q. Lu, Y. Wang, D. Su, Appl. Catal. B Environ. 111–112 (2012) 264–270.
[49] O. Antoine, R. Durand, J. Appl. Electrochem. 30 (2000) 839–844.
[50] S. Sriramulu, T.D. Jarvi, E.M. Stuve, J. Electroanal. Chem. 467 (1999) 132–142.
[51] Y. Takasu, T. Iwazaki, W. Sugimoto, Y. Murakami, Electrochem. Commun. 2 (2000) 671–674.
[52] T. Frelink, W. Visscher, J.A.R. Vanveen, J. Electroanal. Chem. 382 (1995) 65–72.
[53] F. Gloaguen, J.M. Léger, C. Lamy, J. Appl. Electrochem. 27 (1997) 1052–1060.
[54] K. Bergamaski, A.L.N. Pinheiro, E. Teixeira-Neto, F.C. Nart, J. Phys. Chem. B 110 (2006) 19271–19279.
[55] F. Maillard, M. Eikerling, O.V. Cherstiouk, S. Schreier, E. Savinova, U. Stimming, Faraday Discuss. 125 (2004) 357–377.
[56] Y. Takasu, T. Kawaguchi, W. Sugimoto, Y. Muratami, Electrochim. Acta 48 (2003) 3861–3868.
[57] E. Lee, A. Murthy, A. Manthiram, Electrochem. Commun. 13 (2011) 480–483.
[58] L. Chen, G. Lu, Electrochim. Acta 53 (2008) 4316–4323.
[59] B.D. McNicol, P. Attwood, R.T. Short, J. Chem. Soc. Faraday Trans. 77 (1981) 2017–2028.
[60] S.J. Yoo, T.Y. Jeon, Y.H. Cho, K.S. Lee, Y.E. Sung, Electrochim. Acta 55 (2010) 7939–7944.
[61] J. Perez, V.A. Paganin, E. Antolini, J. Electroanal. Chem. 654 (2011) 108–115.
[62] M. Watanabe, H. Sei, P. Stonehart, J. Electroanal. Chem. 261 (1989) 375–387.
[63] O. Antoine, Y. Bultel, R. Durand, P. Ozil, Electrochim. Acta 43 (1998) 3681–3691.
[64] S.H. Joo, K. Kwon, D.J. You, C. Pak, H. Chang, J.M. Kim, Electrochim. Acta 54 (2009) 5746–5753.
[65] P.G. Corradini, F.I. Pires, V.A. Paganin, J. Perez, E. Antolini, J. Nanopart. Res. 14 (2012) 1080–1085.
[66] N. Giordano, E. Passalacqua, L. Pino, A.S. Aricò, V. Antonucci, M. Vivaldi, K. Kinoshita, Electrochim. Acta 36 (1991) 1979–1984.
[67] S. Kumar, S. Zou, Electrochem. Commun. 8 (2006) 1151–1157.
[68] M. Watanabe, S. Saegusa, P. Stonehart, J. Electroanal. Chem. 271 (1989) 213–220.

[69] M. Nesselberger, M. Röefzaad, R.F. Hamou, P.U. Biedermann, F.F. Schweinberger, S. Kunz, K.G. Hartl, G.K.H. Wiberg, S.J. Ashton, U. Heiz, K. Mayrhofer, M. Arenz, Nat. Mater. 12 (2013) 919–924.
[70] J. Speder, L. Altmann, M. Baumer, J.J.K. Kirkensgaard, K. Mortensen, M. Arenz, RSC Adv. 4 (2014) 14971–14978.
[71] E. Fabbri, S. Taylor, A. Rabis, P. Levecque, O. Conrad, R. Kötz, T.J. Schmidt, ChemCatChem 6 (2014) 1410–1418.
[72] H. Yang, S. Kumar, S. Zou, J. Electroanal. Chem. 688 (2013) 180–188.
[73] R.W. Lindstrom, Y.E. Seidel, Z. Jusys, M. Gustavsson, B. Wickman, B. Kasemo, R.J. Behm, J. Electroanal. Chem. 644 (2010) 90–102.
[74] H. Schwechten, M. Heinen, Y.E. Seidel, Z. Jusys, B. Wickman, B. Kasemo, R.J. Behm, J. Electroanal. Chem. 662 (2011) 157–168.
[75] K. Tammeveski, M. Arulepp, T. Tenno, C. Ferrater, J. Claret, Electrochim. Acta 42 (1997) 2961–2967.
[76] S. Kamarajugadda, S. Mazumder, J. Power Sources 183 (2008) 629–642.
[77] J.S. Lee, K.I. Han, S.O. Park, H.N. Kim, H. Kim, Electrochim. Acta 50 (2004) 807–810.
[78] A.L. Dicks, J. Power Sources 156 (2006) 128–141.
[79] E.A. Ticianelli, C.R. Derouin, S. Srinivasan, J. Electroanal. Chem. 251 (1988) 275–295.
[80] T.F. Yang, L.W. Hourng, T.L. Yu, P.H. Chi, A. Su, J. Power Sources 195 (2010) 7359–7369.
[81] M. Mamlouk, K. Scott, J.A. Horsfall, C. Williams, Int. J. Hydrog. Energy 36 (2011) 7191–7198.
[82] T. Suzuki, S. Tsushima, S. Hirai, J. Power Sources 233 (2013) 269–276.
[83] M. Lee, M. Uchida, D.A. Tryk, H. Uchida, M. Watanabe, Electrochim. Acta 56 (2011) 4783–4790.
[84] J. Qi, L. Jiang, M. Jing, Q. Tang, G. Sun, Int. J. Hydrog. Energy 36 (2011) 10490–10501.
[85] Z. Sun, Z. Li, C. Huang, Y. Zhao, H. Zhang, R. Tao, Z. Liu, Carbon 49 (2011) 4376–4384.
[86] M. Umeda, M. Kokubo, M. Mohamedi, I. Uchida, Electrochim. Acta 48 (2003) 1367–1374.
[87] H. Kim, J.N. Park, W.H. Lee, Catal. Today 87 (2003) 237–246.
[88] Y. Xing, J. Phys. Chem. B 108 (2004) 19255–19259.
[89] S. Vengatesan, H.J. Kim, S.K. Kim, I.H. Oh, S.Y. Lee, E.A. Cho, H.Y. Ha, T.H. Lim, Electrochim. Acta 54 (2008) 856–861.
[90] Z. Wang, C.J. Liu, G. Zhang, Catal. Commun. 10 (2009) 959–962.
[91] H. Yano, M. Kataoka, H. Yamashita, H. Uchida, M. Watanabe, Langmuir 23 (2007) 6438–6445.
[92] R. Van Hardeveld, F. Hartog, Surf. Sci. 15 (1969) 189–230.
[93] E. Antolini, F. Cardellini, L. Giorgi, E. Passalacqua, J. Mater. Sci. Lett. 19 (2000) 2099–2103.
[94] E. Antolini, Appl. Catal. B Environ. 88 (2009) 1–24.
[95] V.H. Luan, H.N. Tien, L.T. Hoa, H.L.T. Hien, E.S. Oh, J.S. Chung, E.J. Kim, W.M. Choi, B.S. Kong, S.H. Hur, J. Mater. Chem. A 1 (2013) 208–211.
[96] X.L. Xhou, M. Wang, J. Lian, Y.F. Lian, Sci. China Technol. Sci. 57 (2014) 278–283.